Modelling bowthruster induced flow near a quay-wall

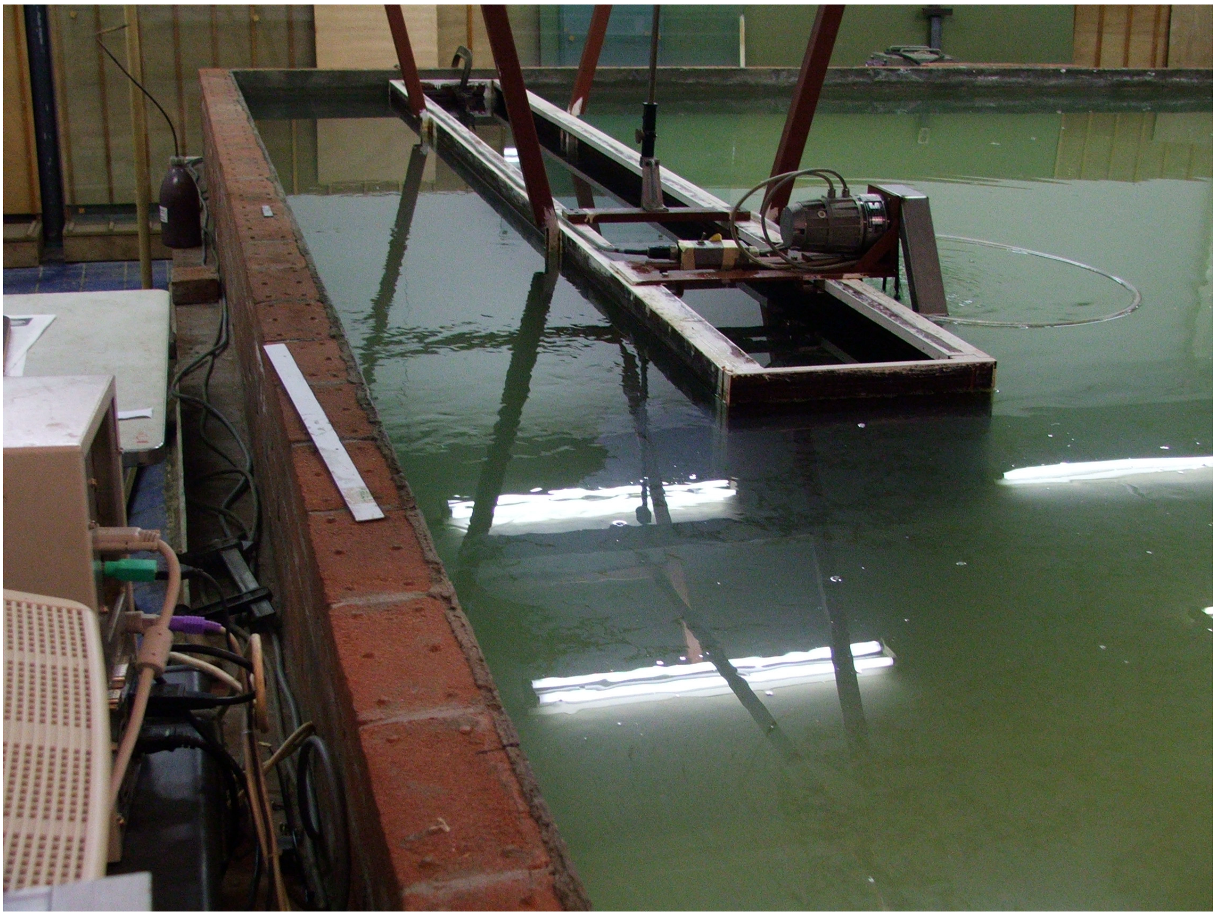

ing. E.A. van Blaaderen, June 2006

The report was established as a Master of Science thesis for Delft University of Technology, under the supervision of a committee with the following members:

prof. dr. ir. M.J.F. Stive
dr. ir. H.L. Fontijn
drs. R. Booij
ir. H.J. Verhagen

Author: ing. E.A. van Blaaderen
Date: June 2006

Preface

As a conclusion of my study at the Delft University of Technology for the department hydraulic engineering, I did an investigation to the usability of a numerical model for calculating bowthruster-induced flow. This report is the result an ongoing research for propeller induced flows at the Delft University of Technology.

For the finalisation of this report, I own a lot of gratitude to many persons. A special thanks to my graduation committee. Their constant guidance and support were of major influence. Besides them, I would like to thank the laboratory staff, for their practical assistance, Mister J. Nefzger, for his efforts to correct my English writing style and my family, for their emotional support.

Egbert van Blaaderen
Ouderkerk aan de Amstel, June 2006

Abstract

For the calculation of bottom protection in harbours near quay-walls, analytical formulas are used. The current experiences suggest an overestimation of load on the harbour bottom. Extensive measurements in prototype situations are very expensive. For this reason, the use of a computer model will be far more economical. However, at this moment there is no expertise in the use of numerical models for this type of situation. For this reason, a physical model was made to validate the use of the numerical model. The results of the measurements of Nielsen were not conclusive, because the two models did not match.

A sensitivity analysis of the numerical model showed that the model is sensitive to changes in the geometry. Especially the changes to the geometry of the bowthruster caused large differences in the calculation results of the model. For the thruster outflow to be modelled accurately, measurements needed to be done in the physical model.

The measurements revealed an unexpected aspect of the flow situation. The low velocity core behind the screw axis was expected to collapse within a certain distance. The measurement results show the core to exist beyond this distance and its contribution to the distribution of the velocities from the bowthruster.

Even though this raises new questions, the adaptations to the bowthruster in the numerical model, reproduced the outflow of the physical model. The calculation results of this model were very comparable to the flow situation measured in the physical model. This gives some confidence for the use of the $k\varepsilon$-model for modelling bowthruster-induced flows. It also shows the importance of modelling the bowthruster. When the outflow of the bowthruster does not match reality, large deviations are expected.

Table of contents

List of figures

Chapter 1: Introduction

In the world of harbour development, there is a growing concern about the consequences of the use of large bowthrusters. To make ships more manoeuvrable, these thrusters are becoming more powerful and are installed on all sizes of ships including the larger ships. This results in an increase of the loads on bottom protections in harbours. With the increasing pressure on economical harbour design, an over-dimensioning of the bottom-protection is a waste of money. However, an under-dimensioning of this protection can result in a collapse of the quay-wall or other structures.

The knowledge of the flow field produced by the bowthruster is limited: Calculating the implications of a bowthruster is not yet possible. There are some rules-of-thumb derived from analytical formulas for free screw propellers but their validity has yet to be confirmed in complex restricted geometries. The objective of this research is to gain knowledge about modelling the bowthruster-induced flow with a numerical model.

Before numerical model can be used to model a mooring situation, the model needs to be validated. For this purpose, a physical model was build by Van der Laan. Measurements in the physical model were done by Nielsen. The comparison between the velocities in the two models, showed a large deviation of the flow situation.

1.1 Problem definition

The difference in these two models was the start of the research for this report. The objective was to adapt the numerical model to the flow situation of the physical model. Before the measurements with an ADV (Acoustic Doppler Velocimeter, see Appendix), the flow situation in the physical model was not fully known. From the measurements of Nielsen, only the velocities close to the bottom were known. The following problems need to be solved:

1. The whole flow situation of the physical model needs to be determined, especially the properties of the bowthruster. A comparison between the numerical and the physical models can show the problem area for modelling bowthruster flow.

2. The sensitive parts of the numerical model on the flow calculations should be mapped. The most sensitive aspects of the model need the most attention for modelling.

3. The numerical model should have the same flow situation as the physical model. Some adaptations of the numerical model are necessary to make a comparison between the two models.

For these objectives to be achieved the following work was done:

First, a parameter analyses was carried out. The values of some used parameters were doubtful. The parameter variation showed which parameters were sensitive to small variations, and which were not.

After this, the flow situation in the physical model needed to be determined. Measurement series were done to measure velocities. The used instrument was the ADV. This was the first time the ADV instrument was used in this research programme. To gain some experience, some measurements were done in a flume. These simultaneous measurements with a LDA (Laser Doppler Anemometer) showed the validity of the measured velocities.

Finally, the flow situation in the physical model was measured. The numerical model could be adapted to the flow situation of the physical model. Some adaptations were also done on the bowthruster, which resulted in a very comparable flow situation.

1.2 Outline of the report

The report is divided in four parts. The first two parts discuss the numerical and physical models, the third part the measurements and the last part the adaptations of the numerical model. The total report is separated into seven chapters.

The first chapter introduces the subject and the background of the report. This chapter is meant to give a global introduction and describes the chronology of the project.

The second chapter contains the state of art. Analytical models and the results of predecessors are described. The analytical models are used in the sixth chapter for comparing the results with some numerical calculations. In addition, the flow situation of the numerical model is described.

The third chapter describes the behaviour of the numerical model. Several parameters are changed to assess their influence and importance to the model. Some of the changed parameters are far fetched, but they can help with assessing other aspects of the model.

In the fourth chapter, the physical model is discussed. Its probable similarity to a prototype situation is assessed on the Froude-number and Reynolds-numbers. The measurement instruments EMS (Electromagnetic Velocity Meter) and ADV, used for measurements in the physical model, are discussed.

Chapter 5 is devoted to the measurements done with the ADV. The choice of the measurement grid is explained and the results are given.

The sixth chapter is an attempt to reproduce the flow situation of the physical model in the numerical model. An adaptation in the geometry of bowthruster resulted in comparable velocity fields. The similar outflow of the bowthruster in both models gives some confidence that the model will also produce good results in other geometries.

The last chapter contains conclusions and recommendations of the research done for this report.

Chapter 2: State of art

This chapter describes the present knowledge other researchers gathered in the past. Some analytical models are discussed. After this, the research done on the development of the numerical model is described. The definition of the coordinate system defines the axis and directions used in the physical and numerical model. Because the researchers on the numerical model did not give a full description of the bowthruster induced flow situation, this will be the final part in this chapter.

2.1 Earlier research

Some research has already been done on bowthruster-induced flows. The formulas for normal propeller-flow were used to model the generated velocities. The models are widely used for all kinds of ship-related flow calculations. There is some doubt about the usability of these formulas for calculations in confined conditions as bowthruster induced flow. Besides this, thorough investigations of their validity and limitations are not yet done.

2.1.1 Analytical model

There is a variety of different formulas for modelling the bowthruster flow against a vertical quay-wall. Verheij and Römisch derived the first formulas. However, these models are hardly used anymore. Schmidt and Blokland made improvements on them. These formulas are discussed below.

Blokland (1994)

Blokland did some prototype tests of propeller flow against a vertical quay-wall. The bowthruster and ship were substituted by a tugboat with the same power on the main thrusters as a large container vessel has on the bowthruster. From these tests, he derived relations for the maximum bottom velocities and stability of the bottom protection in front of the quay wall.

The relations for the flow velocities close to the bottom are:

$$U_{b;\max} = 2.8 \frac{U_0 \cdot D_b}{L + h_p} \text{ [m] for } \frac{L}{h_p} \geq 1.8 \text{ [-]} \tag{2.1}$$

$$U_{b;\max} = 1.0 \frac{U_0 \cdot D_b}{h_p} \text{ [m] for } \frac{L}{h_p} < 1.8 \text{ [-]} \tag{2.2}$$

where:

$U_{b;max}$ = maximum velocity on the bottom [m/s]
U_0 = axial screw velocity [m/s]
L = distance between the outflow of the bowthruster and the quay wall [m]
D_b = diameter of the bowthruster [m]
h_p = height of the bowthruster axis above the harbour bottom [m]

The axial screw velocity is the average velocity of the flow through the bowthruster along the rotation axis of the screw.

The tests of Blokland are the only experiments done on a prototype scale. The validity for substituting the vessel with bowthruster by a tugboat is doubtful. This suggests that the influence of a ship should be very small, for this to be true. One of the differences is the flow outside the diameter of the tugboats screw. The bowthruster only has a flow through the screw. The total flow rate from the propeller of the tugboat is higher then from a bowthruster with the same diameter. The calculations with the formula's of Blokland can here for be seen as an overestimation of the real load on the harbour bottom.

Schmidt (1998)

Other analytical formulas were suggested by Schmidt. His formulas were directly derived from the knowledge of screw-flows of Römisch and validated with some measurements in a physical model. They are based on the assumption that a bowthruster can be modelled as a free propeller, with some different constants.

Analytical formulas Schmidt:

For calculating the erosion velocities at the bottom, the formulas below are used.
The maximal vertical velocity at the quay-wall:

$$U_{wa;\max} = 1{,}9 \cdot \left(\frac{L}{D_b} \right)^{-1{,}0} \cdot U_0 \quad \text{and } U_{wa;\max} < U_0 \tag{2.3}$$

The maximum vertical velocity on the bottom is calculated with:

$$U_{wa;b} = 10.6 \cdot \left(\frac{L}{D_B} \right)^{-1.0} \cdot \left(\frac{h_p}{D_B} \right)^{-1.15} U_{wa;\max} \quad \text{and } U_{wa} < U_{wa;\max} \tag{2.4}$$

where:
$U_{b;max}$ = maximum velocity at the harbour bottom [m/s]
$U_{wa;max}$ = maximum velocity at the wall [m/s]
U_0 = axial screw velocity [m/s]
L = distance between the outflow of the bowthruster and the quay wall [m]
D_b = diameter of the bowthruster [m]
h_p = height of the bowthruster axis above the harbour bottom [m]

The formulas of schimdt are extendable to calculate the bowthruster induced flow field. Here it becomes clear which assumptions are made for the two regions. The free screw formula 1.3 is valid for the first 0.7 times the distance between the ship and the wall, and the wall distribution formula (formula 1.4) is valid for the 0.3 times this distance. This results in the following relative flow field of the modelled situation:

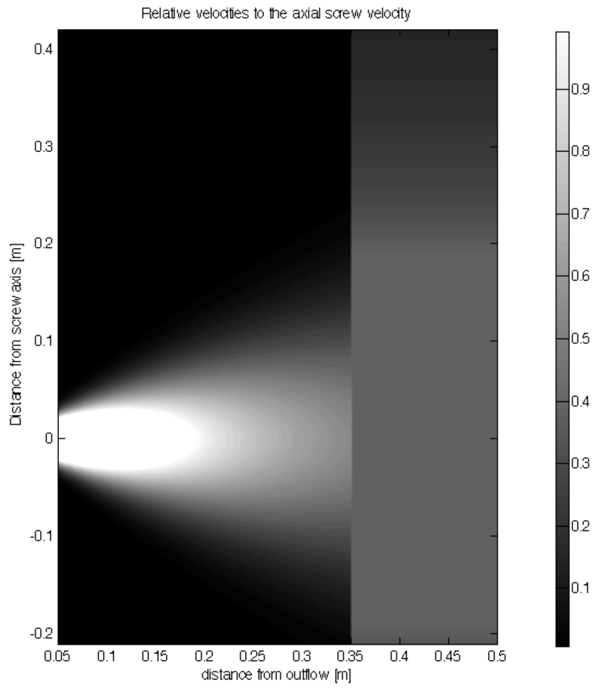

Figure 1: Visualisation of the relative analytical flow field Schmidt

Clearly visible is the assumption of the flow distribution of the screw. Normally, behind the propeller a low-velocity core is expected from the presents of the screw axis in the propeller. This low velocity core is not modelled. In free propeller flows, this is not necessary. The core disappears after some distance of the propeller. Modelling this aspect was assumed to be of no interest for the bowthruster flow.

The analytical models in the situation of the physical model

To summarise, the analytical models and their values for the maximum bottom velocities can be calculated for the geometry of the physical model. The maximal horizontal velocity on the bottom is assumed equal or proportional to the axial screw velocity. This is the basis of the analytical models. For comparing the results, it is better to calculate relative bottom velocities. This way, the analytical models, numerical calculations and measurements in the flume can be compared to assess there validity.

Analytical model	Maximum bottom velocity ($U_{b;max}$) [m/s]		Relative maximum bottom velocity [-]
	U_0 = 0.45 m/s	U_0 = 1.60 m/s	
Blokland (1994)	0.18	0.63	0.394
Schmidt (1998)	0.15	0.55	0.343

Dividing the maximum bottom velocity through the axial screw velocity, the relative maximum bottom velocity is calculated. The models of Schmidt and Blokland and the formulas of the numerical model suggest a fixed relative maximum bottom velocity value in a fixed geometry. This aspect can be used to show the differences between the models in chapter 6.

2.1.2 Van der Laan (2005)

Van der Laan build a physical scale model to assess if a CFD (Computational Fluid Dynamics) -model with turbulence can be used for calculating the complex flow situation of a mooring ship. His predecessors (Schokking (2002) and De Jong(2003)) already concluded that the bowthruster could not be modelled as a jet-flow. The rotation is of great importance on the flow field.

With this knowledge, Van der Laan chooses a situation for a physical model in the laboratory. In addition to this model, he also made a numerical model. With the numerical model, he assessed the influences of the walls. The dimensions of the physical model were chosen to have a minimum influence of the sidewalls on the flow situation. The comparisons he made between the models were based on a very limited number of measurement points. However, from this data it shows that the calculated and measured situations were not within the limits of the expected values.

Van der Laan copied the settings of the bowthruster from the results of De Jong's research. He did not check the outflow of the bowthruster in the physical model. For this reason, it could happen that the real flow rate in the physical model was far lower as assumed on the calculations of the screw.

2.1.3 Nielsen (2005)

As a follow-up on the work of Van der Laan, Nielsen made a series of measurements for one flow-situation in the model of Van der Laan. He measured the flow field at 0.03 m above the bottom with a tracer and an EMS instrument. This height is half the keel clearance underneath the ship. From his data series, it shows very clearly that the calculated and measured flow fields deviate substantially. However, the origin of the differences was not clear.

There were some doubts on the measurements with the EMS. This was partially related to the instrument. The measurement volume and instrument were large compared to the flow situation. In the confined space of the keel clearance, under the ship, the instrument is relative large. This could result in higher measured velocities, because the flow needed to flow around the instrument. At other places, the calculations predict a substantial vertical velocity. What the instrument does with the vertical velocity components is unknown. Besides all these remarks, the measurements done with the EMS partially comply with the visual measurements.

The results of both measurements are giving below. (A description of the orientation of the coordinate system is in the next paragraph)

Measurements from Nielsen (2005):

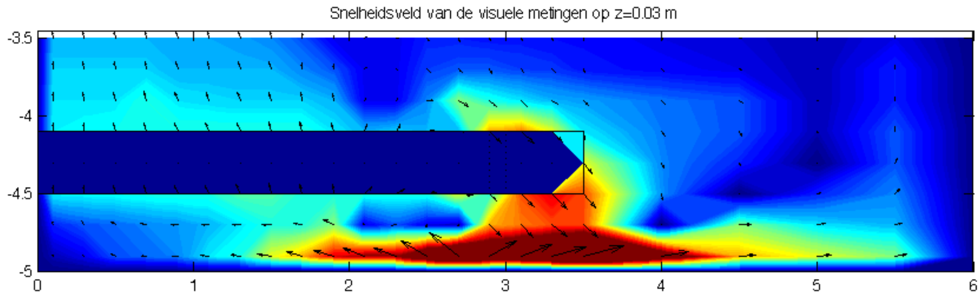

Figure 2: Results of the visual measurements of Nielsen (2005) on z = 0.03 m

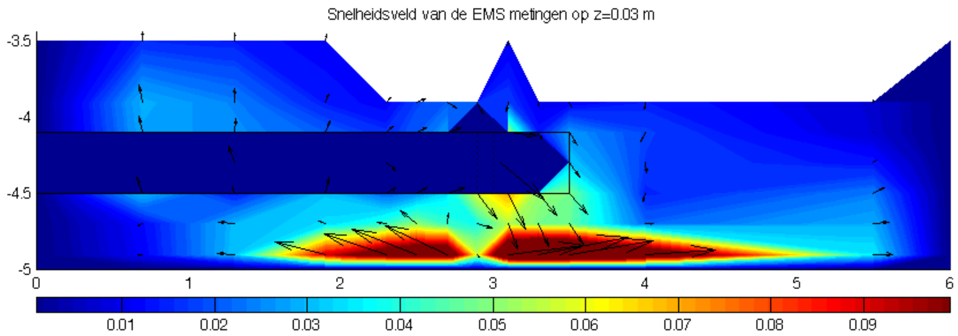

Figure 3: Results of the EMS-measurements of Nielsen (2005) on z = 0.03 m

2.2 Definition of the coordinate system in the models

The coordinate system in the model is the same for the physical model and the numerical model. All coordinates in this report are on this coordinate system. The deviation is given below the figures if this is not true. The origin is placed in the far corner on the bottom of the basin. The picture below shows the corner and the positive direction on each axis.

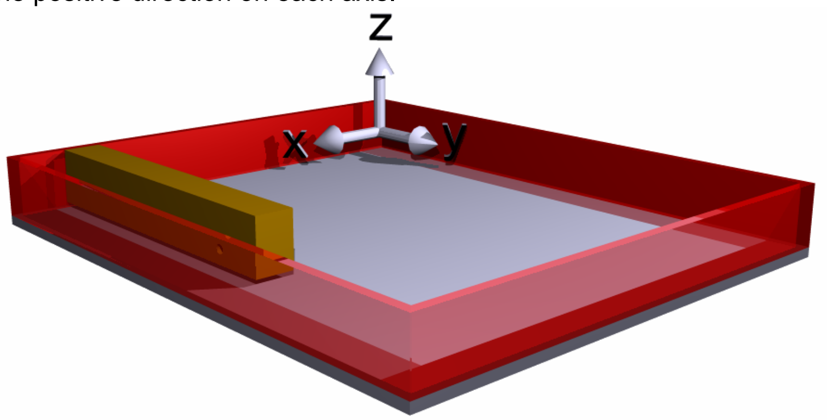

Figure 4: Definition of the coordinate system

The basin was 6.0 m along the quay-wall and 5.0 m perpendicular to it. The model of the ship is a simplified version of the containership “pride of Rotterdam”. This ship was used to have comparable relative dimensions to real-life situations. The positioning of the ship in the model is chosen for easy measurements of the situation. The bow of the ship is simplified to the shape of a block. Numerical calculations and the production of the physical model are easier with a simple geometry. This all gives us the dimensions as given in the table below.

Object	**Prototype scale**	**Model scale**	
Dimensions of the flume			
Length		6.00 m	
Width		5.00 m	
water depth	15.75 m	0.63 m	
Ship			
length	215 m	8.60 m	(shortened to 3.50 m)
Width	30 m	1.20 m	(narrowed to 0.40 m)
Draft	14.25 m	0.57 m	
diameter bowthruster	2.5 m	0.10 m	
distance bowthruster axis from the bow		0.55 m	
distance bowthruster axis from the keel	3.75 m	0.15 m	
length of the thruster tunnel	8.7 m	0.35 m	(widened to 0.40 m)
Positioning of the ship			
Distance between the quay wall and the ship	12.5 m	0.50 m	
Keel clearance	1.5 m	0.06 m	

The dimensions of the ship and its positioning in the basin are given in the picture below.

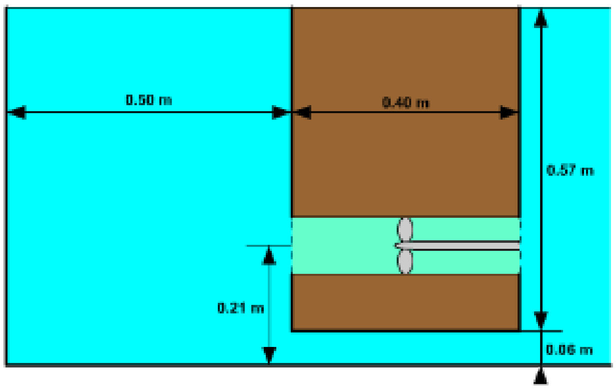

Figure 5: Cross section to show the positioning and dimensions of the ship

Van der Laan chose these dimensions. He made some calculations with different basin sizes of the basin. This size of the model was chosen for a minimal influence of the basin sidewalls on the flow situation. In most real-life situations, the only wall present is the quay wall.

2.2.1 Original calculations

The original calculations are from the numerical model made by Van der Laan. Nielsen used the same model to compare it with his measurements in the physical model. They both used the model, but did not describe the flow field. Therefore, there is a description of the flow field in this section. The calculations of Van der laan and Nielsen were slightly different. The difference between the models is the size of the calculation grid. Besides this difference, the calculated flow field was the same.

Screw propeller
The source of all flow in the model is the propeller in the bowthruster. In the numerical model, the outflow is almost uniform. Only the effect of the rotation of the screw propeller is still noticeably present. This is partly in line with the analytical model of Schmidt. Only the very low diffusion of the velocity distribution is different from his model. The low diffusion rate gives a very concentrated flow area on the wall.

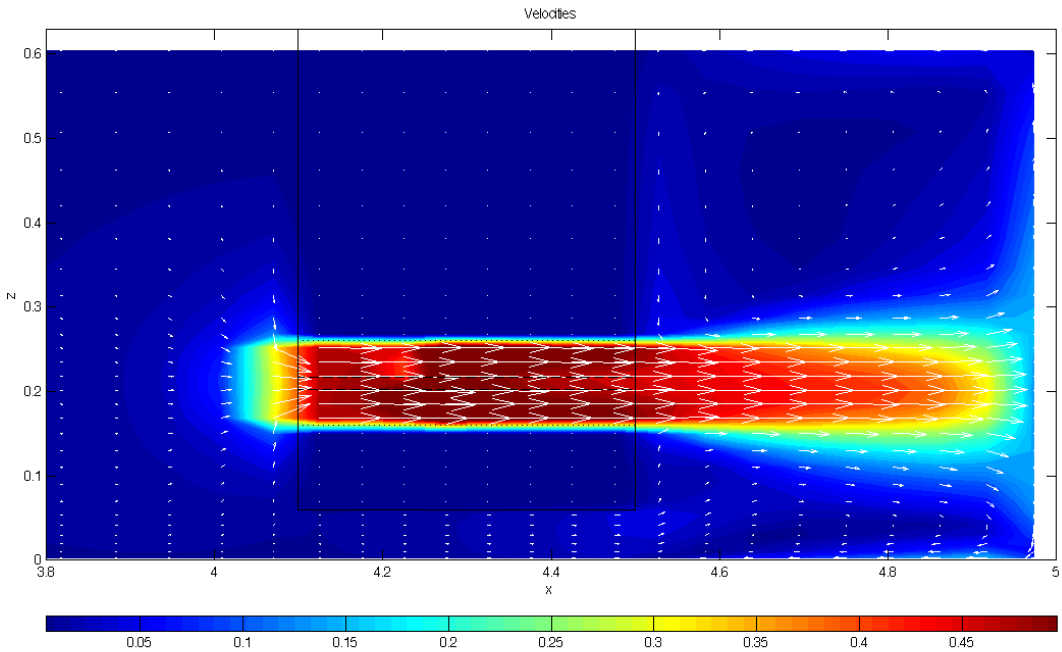

Figure 6: Numerical bowthruster on y = 2.95 m

The implications of the propeller flow on the bottom are given below. The water jet bounces on the quay-wall and produces an almost symmetrical velocity-distribution close to the bottom. The hindrance of the ship is very low, because the flow is very close to the bottom.

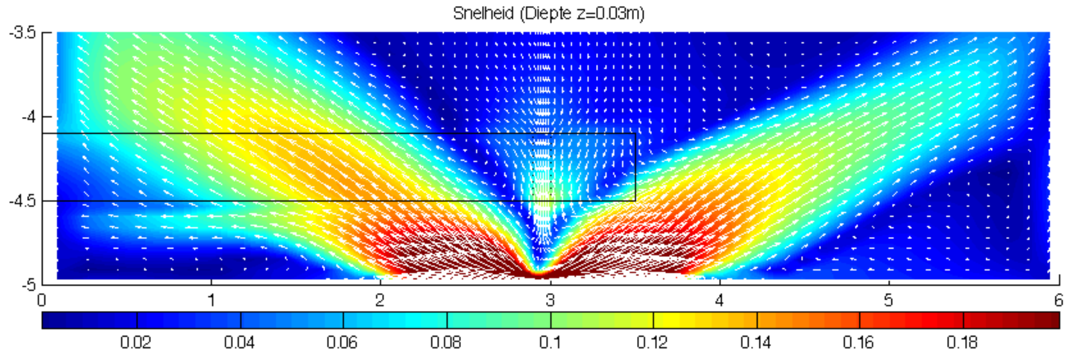

Figure 7: Horizontal flow field at 0.03 m above the bottom on z = 0.03 m

Nielsen used the velocity field of this location for comparing the measurement results with the numerical calculations. The further implication for the three-dimensional flow situation is not assessed. It gets more interesting when vertical cross sections of the flow field are made, for instance perpendicular to the length of the ship.

As shown in Figure 7, there are locations under the ship where the flow has two layers, with an opposite flow directions over the vertical. This could be interesting to measure, as the production of turbulent energy on these locations would be severe and have a large influence on the stability of the bottom protection. Also noticeable is the creation of vortices. These are driven by the rotating flow of the bowthruster. Because of this flow, the vortices have a rotational character and orientation.

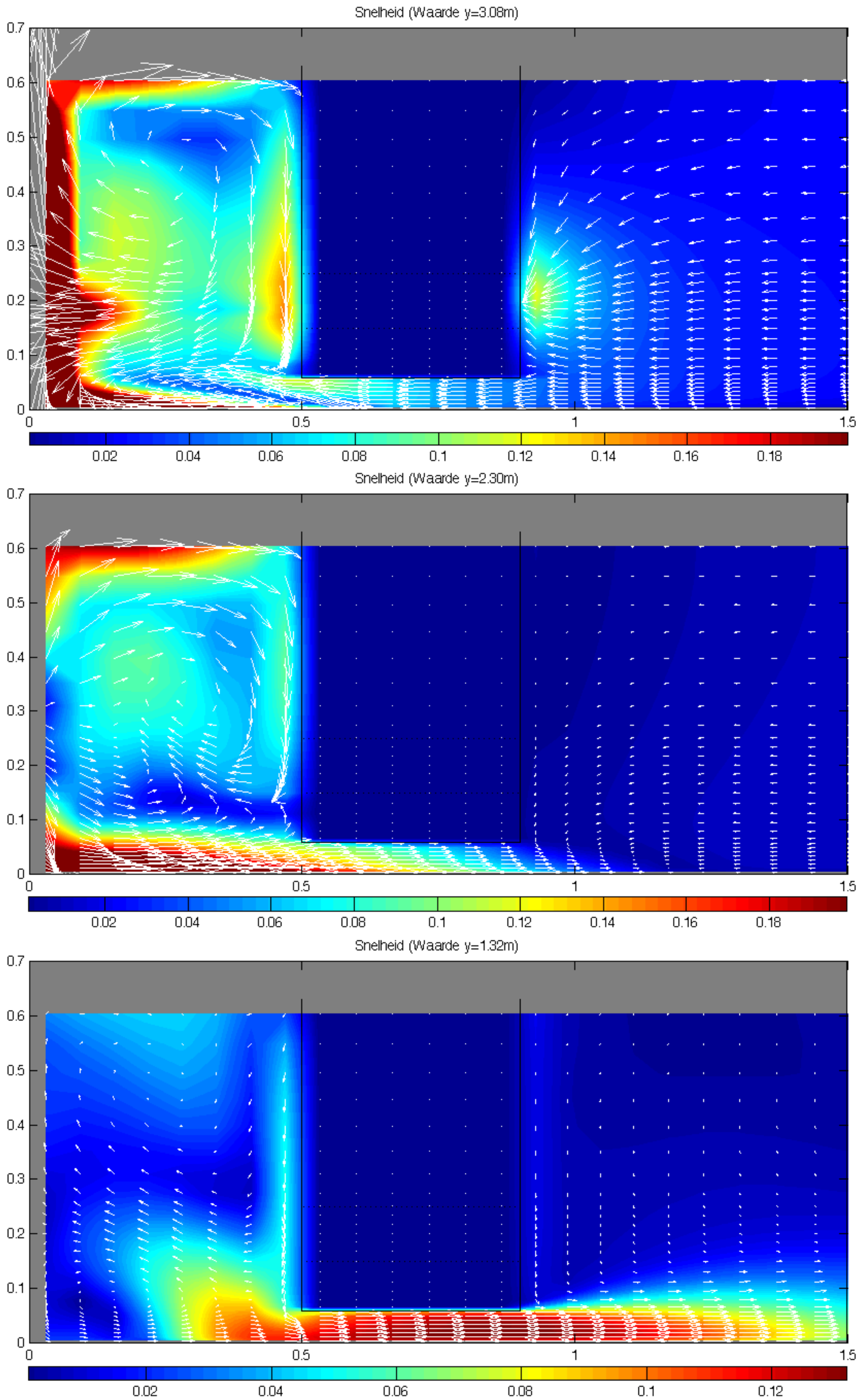

Figure 8: Vertical cross section of the flow field on y = 3.08, 2.30 and 1.32 m

(x-coordinates give the distance from the quay wall)

The vertical cross sections of the velocity field parallel to the ship are also interesting. The rotating flow of the propeller flow of the bowthruster produces some vortices. They are strengthened or subdued by the rotation of the propeller flow, but they are stable due to the vicinity of boundaries as the surface and the bottom. They make a strong downwards current on the side of the ship. They also push the main part of the reflecting flow to the bottom and the water surface. This is in contradiction to the analytical formulas of Schmidt. He assumes a radial distribution of the flow-velocities, not a flow bound to the walls by vortices.

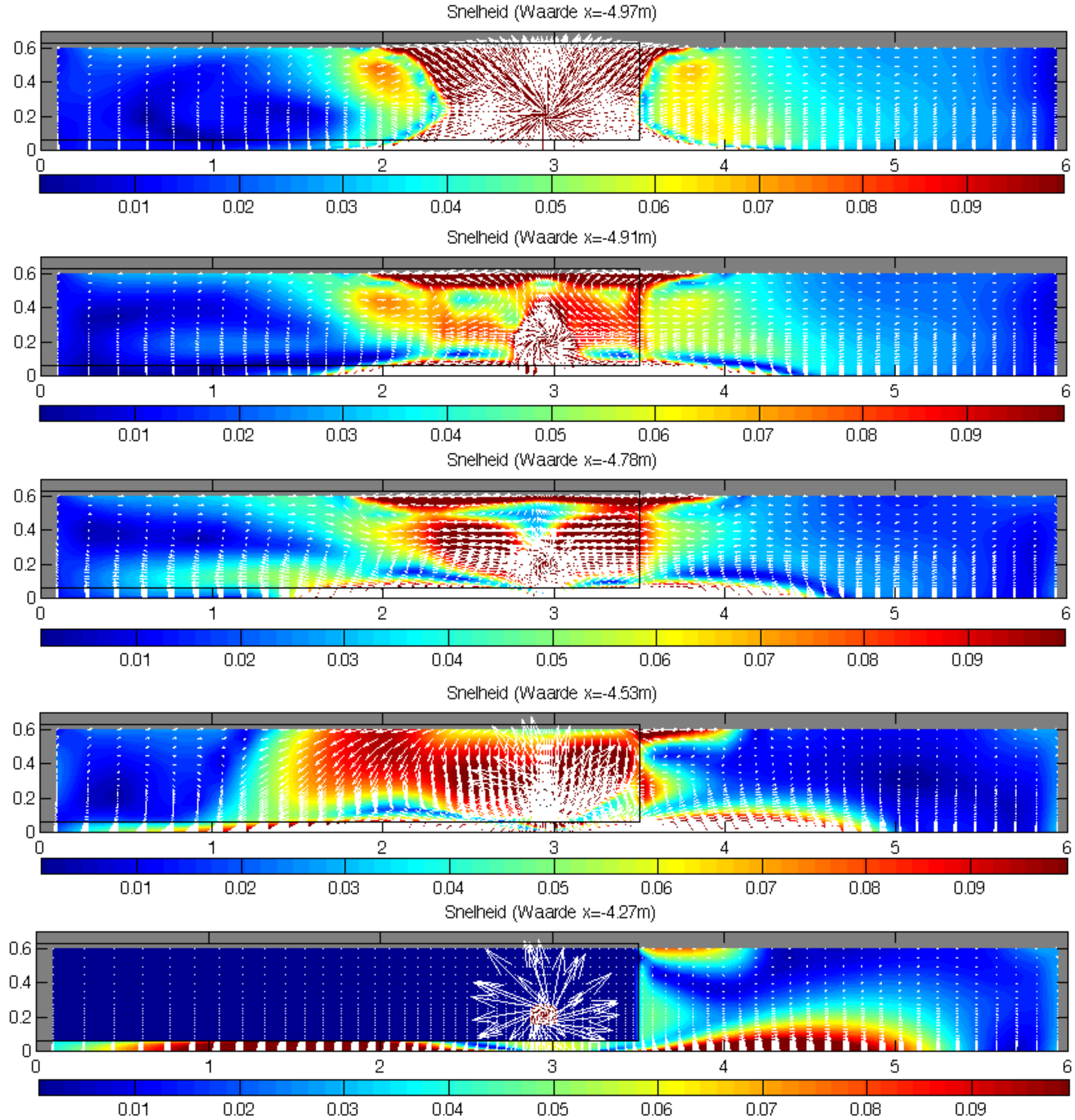

Figure 9: Longitudinal cross sections of flow situation between the quay-wall and the ship on x = 4.97, 4.91, 4.78, 4.53 and 4.27 m

Chapter 3: Behaviour of numerical model

This chapter discusses the numerical turbulence model. First, the formulas are described. After this, a sensitivity analysis is done on the physical model. The whole chapter gives an impression of the capabilities of the numerical model and its relation to the flow conditions in real-life.

3.1 Model definition

3.1.1 Turbulence model

The used turbulence model in the numerical calculations is the kε-model. The kε-model is a viscous turbulence model for modelling turbulent flows. The model is widely used for flow calculations. Of this model is known that the calculation results in high-turbulent flow conditions are quite good. Because the expected flow in the model is highly turbulent, the use of this turbulence model is assumed to be justified.

De Jong (2003) validated the model for the modelling of a propeller flow. He used the research on propeller flow of Veldhoven (2002) and Schokking (2002) for the validation of the numerical model. He concluded that for correct modelling of the flow, it is necessary to model the swirling motion of the jet. To model the swirl correctly, he proposed to use 0.8 times the axial screw velocity for the rotational velocity of the propeller flow.

Description of the kε-model

For the calculations of high turbulent flows the standard kε-model can be summarised as follows:

$$\frac{\partial \rho k}{\partial t}+\frac{\partial}{\partial i}\left(\rho U_i k-\left\{\frac{\rho \nu_{eff}}{\sigma_k}\right\}\frac{\partial k}{\partial i}\right)=\rho\left(P_k-\varepsilon+G_b\right) \tag{3.1}$$

$$\frac{\partial \rho \varepsilon}{\partial t}+\frac{\partial}{\partial i}\left(\rho U_i \varepsilon-\left\{\frac{\rho \nu_{eff}}{\sigma_\varepsilon}\right\}\frac{\partial \varepsilon}{\partial i}\right)=\left(\rho\frac{\varepsilon}{k}\right)\left(C_1 P_k-C_2\varepsilon+C_3 G_b\right) \tag{3.2}$$

$$\nu_t=C_\mu\frac{k^2}{\varepsilon} \tag{3.3}$$

$$\nu_{eff}=\nu_t+\nu \tag{3.4}$$

where:

ρ = density [kg/m^3]
k = turbulent kinetic energy [J/m^3]
ε = dissipation of turbulent energy [-]
U_i = flow velocity in the flow direction i [m/s]
ν_{eff} = turbulent kinetic viscosity [m^2/s]
ν_t = turbulent kinetic viscosity [m^2/s]
ν = molecular viscosity [m^2/s]
σ_k = turbulent Prandtl constant (1,0) [-]
σ_ε = turbulent Prandtl constant (1,314) [-]
P_k = production of turbulent kinetic energy by shear stresses per volume:

$$P_k=\nu_t\left(\frac{\partial U_i}{\partial j}+\frac{\partial U_j}{\partial i}\right)\frac{\partial U_i}{\partial j} \tag{3.5}$$

C_1 = a constant (1,44)
C_2 = a constant (1,92)
C_3 = a constant (1,0)
$C\mu$ = a constant (0,09)
G_b = reduction of turbulent kinetic energy production by density differences (=0)

The model is only applicable with high Reynolds numbers. This means that the model needs specialised functions to calculate the turbulence near walls. The Reynolds numbers are here too low. The use of the turbulence is not valid for modelling.

It is known that in several cases the model is less usable, as the model often produces deviating results from reality. These cases are:
- Separated flows;
- Strong buoyancy;
- Some streamline curvatures;
- Swirl;
- Turbulence-driven secondary flows;
- Rotation;
- Compressibility;
- Adverse pressure gradients;
- Axis-symmetrical jets;

For several cases, ad-hoc relations can be used to correct for the shortcomings of the kε-model. The kε-models of Lam-Bremhort and Chen-Kim are examples of this kind of corrections. Although these models are widely used, they are empirical adaptations for the standard kε-model. There physical background is very doubtful.

3.1.2 Logarithmic wall-functions

For calculating the flow near the walls, the kε-model is not applicable. Here there are some assumptions made to calculate the influence of the walls. The flow at the boundary is assumed to be of a logarithmic shape. From this assumption, the production and dissipation of turbulence is calculated. These logarithmic wall-functions are widely accepted to be correct in almost all cases.

In the modelling software Phoenics, there are three different wall-functions included. Phoenics is the name of the numerical software used for calculating the numerical model. All of these functions are logarithmic wall-functions. They use the roughness of the wall to calculate the turbulence production and dissipation.

Equilibrium logarithmic wall-function

The most used wall-function is the equilibrium wall-function. It assumes equilibrium in the exchange of impulse at the wall. This is true when the flow is stationary.

$$\frac{U}{u_\tau} = \frac{\ln\left(Ey^+\right)}{\kappa} \tag{3.6}$$

with $u_\tau = \sqrt{\frac{\tau_w}{\rho}}$ **(3.7)**

and dimensionless distance $y^+ = \frac{u_\tau y}{\nu}$ **(3.8)**

$$k = \frac{u_\tau^2}{\sqrt{C_\mu}} \tag{3.9}$$

and $\varepsilon = C_\mu^{0,75} * \frac{k^{1,5}}{\kappa y}$ **(3.10)**

where:

U	= absolute velocity parallel to the wall in the first grid point from the wall [m/s]
u_τ	= shear stress velocity [m/s]
E	= roughness parameter [-]
κ	= Von Karman constant [-]
k	= turbulent kinetic energy [J/m^3]
ε	= dissipation of turbulent energy [-]
y	= distance from the first grid point to the wall [m]
ν	= molecular viscosity [m^2/s]
τ_w	= wall shear stress friction N/m^2
ρ	= density [kg/m^3]
C_μ	= closure coefficient [-]

Strictly, the value of y^+ must be between 30 and 130 to be valid. When this model is used, this must be checked.

General logarithmic wall-function

There is also a generalised version of the equilibrium wall-function for the non-equilibrium cases. This wall-function was presented by Launder and Spalding (1974).

$$\frac{U \cdot \sqrt{k}}{u_\tau^2} = \frac{\ln\left(E_s \sqrt{k} \frac{y}{\nu} \right)}{\kappa_s} \qquad (3.11)$$

where:

$$\kappa_s = \kappa \cdot C_\mu^{0,25} \qquad (3.12)$$

$$E_s = E \cdot C_\mu^{0,25} \qquad (3.13)$$

The general wall-function uses $\sqrt{k}$ as characteristic for the turbulent velocity-scale instead of, the turbulent shear stress velocity (u_τ).

The value of turbulent kinetic energy *(k)* in the cells at the wall is calculated with a separated transport equation. The diffusion of turbulent energy through the wall is assumed to be zero. This transport equation includes a production term P_k and dissipation speed ε. The average of these two values for the boundary cell is determined with an analytical integration over the control volume, with the assumed shear stresses and turbulent kinetic energy *(k)* as constant over the cell. The average value of production of turbulent kinetic energy (P_k) is given by:

$$P_k = \frac{u_\tau^2 U}{2y} \qquad (3.14)$$

The average turbulent energy dissipation speed at the cell boundary is:

$$\varepsilon = C_\mu^{0,75} k^{1,5} \frac{\ln\left(E_s \sqrt{k} \frac{y}{E_0} \right)}{2 A_k y} \qquad (3.15)$$

Equivalent roughness parameter (E)

The roughness parameter can be calculated with the formulas of Jayatilleke (1969). The sand grain size is used to calculate, with the flow conditions, a dimensionless roughness value (E). The wall Reynolds number (Re_w) represents the flow conditions near the wall. This parameter is used to make the roughness value dimensionless. Because there are different types of wall flow, there is a different formula for each type of boundary flow taking in to account the implications on the wall-friction.

$$\mathrm{Re}_w = \frac{u_\tau \cdot d}{\nu} \qquad (3.16)$$

for $\mathrm{Re}_w < 3.7$: $E = E_m$ (laminar wall-flow)

for $3.7 < \mathrm{Re}_w < 100$: $E = \dfrac{1}{\sqrt{a\left(\frac{\mathrm{Re}_w}{b}\right)^2 + \left(\frac{1-a}{E_m^2}\right)}}$ (transition wall-flow)

for $\mathrm{Re}_w > 100$: $E = \dfrac{b}{\mathrm{Re}_w}$ (turbulent wall-flow)

where:

Re_w = Reynolds number at the wall
d = Equivalent sand grain roughness height
$\mathrm{E_m}$ = Constant for smooth wall (= 8,6)
b = Constant (= 29,7)
a = $1 + 2X^3 - 3X^2$
X = $0{,}02248 \dfrac{100 - \mathrm{Re}_w}{\mathrm{Re}_w^{0{,}0564}}$

Fully rough wall-function

The last function is the fully rough wall function. It is used for the calculation of fully rough wall flow. This means the flow conditions near the wall are highly turbulent, regardless the flow velocities or wall Reynolds numbers. This wall-function assumes a local equilibrium in the forces, given by:

$$\frac{U}{u_\tau} = \frac{\ln\left(\frac{y}{y_0}\right)}{\kappa} \qquad (3.17)$$

where:

y_0 = effective roughness height

The effective roughness height is related to the size of the roughness elements on the surface.

3.2 Description of the bowthruster

De Jong (2003) researched the parameters and dimensions of the bowthrusters. He suggested, based on the measurements of Schokking, the geometry of bowthruster. The bowthruster was modelled as a propeller in a pipe. The propeller had a few parameters: the axial screw velocity, the rotational ratio and the size of the axis plate. The axial screw velocity is the average flow velocity through the bowthruster along the direction of the screw axis.

The second parameter was to model the rotational character of the flow. It describes a rotational ratio between the axial screw velocity and the rotational velocity of the propeller flow. From the measurements of Schokking, De Jong concluded this to be 0.8 for the used screw.

The third parameter was the size of the axial screw plate. The numerical model was found to produce a wrong velocity distribution at the outflow of the ducted propeller. De Jong suggested that enlarging the size of a centre plate, which substituted the screw axis, could repair this behaviour of the model. He found that a centre plate with a diameter of 30% of the bowthruster diameter to be sufficiently large.

3.3 Sensitivity analyses of the numerical model

To show the importance of different parameters in the flow model several calculations are made. The influence of different roughness parameters is expected to be important for the flow field. Also, checks are made for the change of turbulence model, laminar viscosity and some geometrical dimensions. A list of the changed parameters is given below.

Parameter	***Remarks***
turbulence model	Calculations are made with different turbulence models. adapted kε-models of Chen-Kim and Lam-Bremhorst and the kω-model of Wilcox are used
wall friction	The wall roughness was changed on the value of sand-grain roughness. Different roughness values were used on the bottom, quay-wall and ship.
molecular viscosity	The molecular viscosity value is changed. Physically this is not correct. This value is a property of the fluid. However, the turbulence is modelled as a viscosity. So increasing the value of the viscosity can also be explained as an assumption of a minimum value of turbulence in the numerical model.
bowthruster flow rate	An attempt is made to increase the velocities in the numerical model
Geometrical parameter	
keel clearance	The influence of the keel clearance on the asymmetry of the flow on the bottom will be shown.
water depth	The influence of a lower water level.
bowthruster diameter	This was done to increase the velocities in the model.

3.3.1 Another turbulence model

The use of the kε-model is only possible if the flow in the model is highly turbulent. The scaling of the physical model could have reduced the turbulent flow in the physical model. Calculations were made to see if this scaling problem results in a wrong calculated flow field. Part of these calculations was the calculation on prototype-scale. The results did not deviate from the calculations of the physical model. From the formulas of the turbulence model, this was expected; however, the wall functions could still have some influence.

Then, the model calculations were made with low-Reynolds-number turbulence models. The adapted kε-models of Chen-Kim and Lam-Bremhorst and the kω-model of Wilcox are used. All turbulence models resulted in similar flow fields. There were small deviations but they were not substantial. To show this, the results of the calculation with the standard kε-model and the kε-model of Chen-Kim are visualised below.

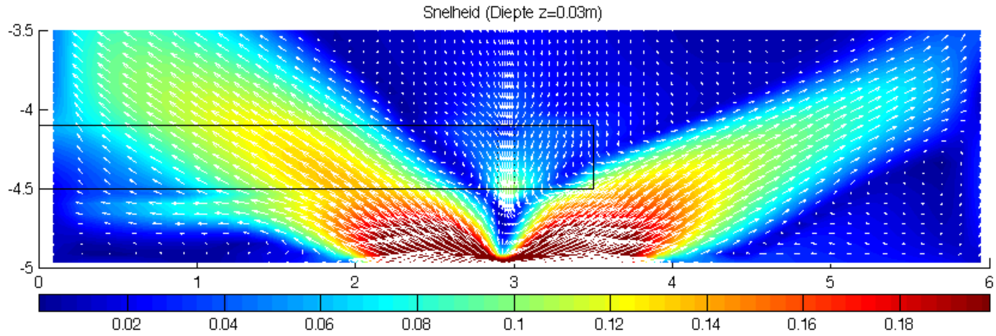

Figure 10: Calculated flow field with standard kε-model on z = 0.03 m

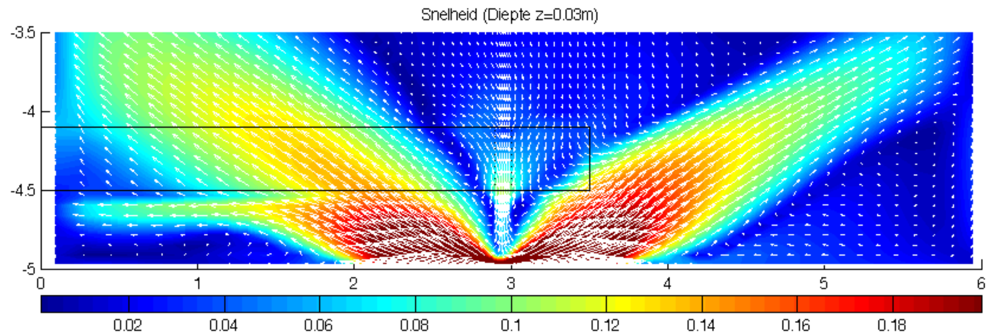

Figure 11: Calculated flow field with kε-model of Chen-Kim on z = 0.03 m

From the results of these calculations it shows that, there is no influence of low turbulent conditions in the calculations. It also gives some confidence of the applicability of the standard kε-model for the calculating the physical model. However, the shortcomings of the models with relation to the assumption of isotropic turbulence are hereby not checked. All the models used in this comparison have this assumption.

3.3.2 Influence of wall-friction on the flow situation

Some of the more important parameters are the wall-friction coefficients. In many flow situations, they are capable of fully determining the flow field. In our model, they are assumed to be of less importance, because the turbulent flow is produced in a single source. The expected turbulent energy levels are much higher as they could be due to wall-friction.

Nielsen (2005) concluded that the wall-friction in the numerical model was to low. The walls in the model were set to be hydraulically smooth. He suggested different boundary conditions were the key for a better comparison. Mainly because he measured far slower velocities under the ship as was expected from the calculations.

Redefining the wall conditions can be done with a wall-function that takes in account the roughness of the walls. A first estimate of the rough elements on the walls is that it will be of the order 1 mm. With the equivalent sand grain roughness formulas of Jayatilleke (1969), the roughness parameter is calculated. Using this roughness the influence of the walls is only noticeable under the ship. There is almost no difference with the calculations where the walls were modelled as hydraulically smooth (Figure 12 and Figure 13).

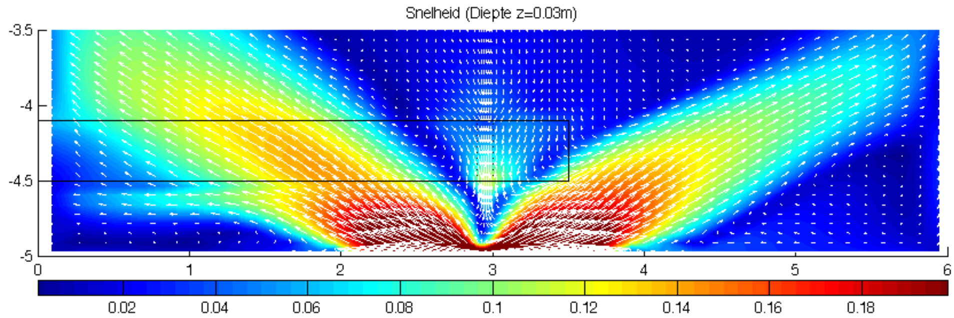

Figure 12: Calculated flow field with smooth walls on z = 0.03 m

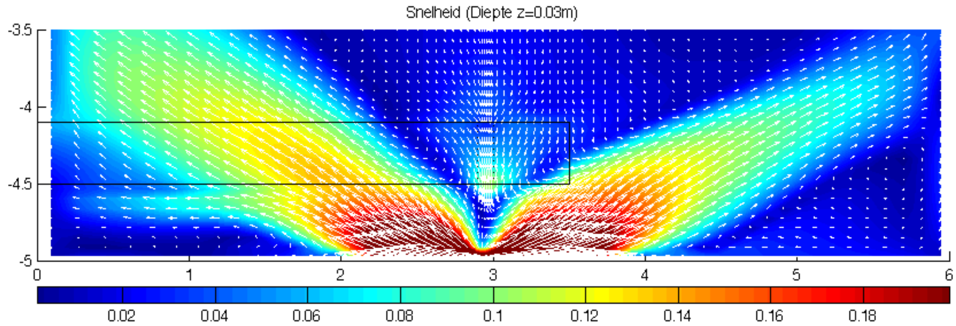

Figure 13: Calculated flow field with rough elements of 1 mm on z = 0.03 m

An attempt was made to reproduce the measurements of Nielsen (2005) in a calculation by changing the roughness of the different wall elements. This resulted in physically not feasible values for the wall roughness (Figure 14 and Figure 15). A roughness size of 5 m was used in the available spaces of 0.06 m. Besides this, the result was still not the same on the measurement locations of Nielsen in the physical model. The largest deviations were at the location where the propeller flow hits the quay wall. The measured velocities are at this location far lower as expected form the calculations.

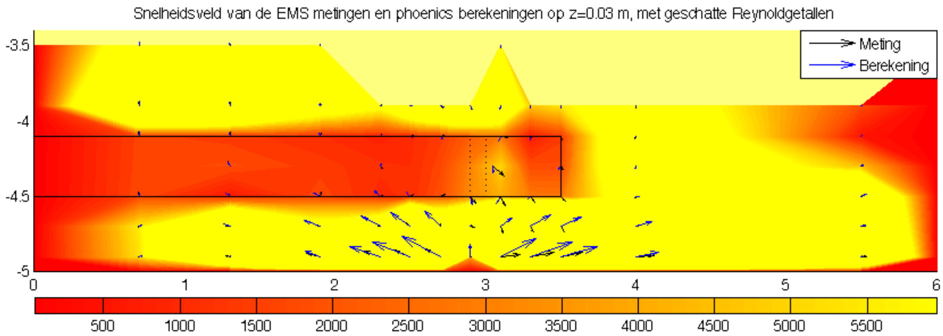

Figure 14: Comparison between the flow field of the calculations (berekening) (with adapted roughness) and the EMS measurements (meting) by Nielsen (2005). The background is coloured with the estimated Renolds values of the flow, given the measured velocity and shortest distance between the restricting elemtents on z = 0.03 m.

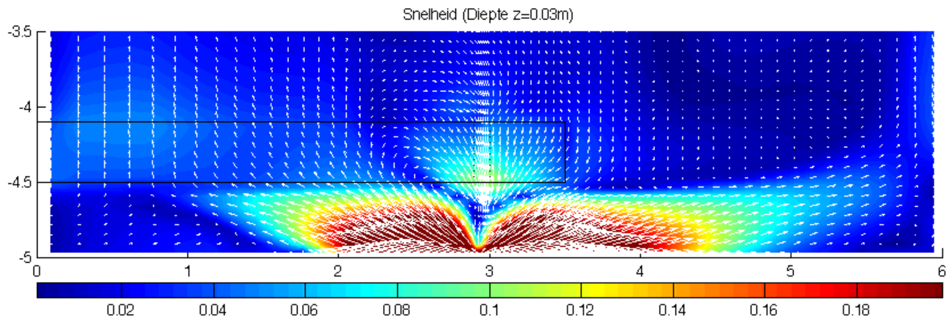

Figure 15: Calculated flow field with a composition of different roughness values on the different wall elements (atempt to reproduce the measured flow field of the EMS) on z = 0.03 m

From this, the conclusion was drawn that changing wall roughness parameters will not be fully satisfying in reproducing the EMS measurements with calculations. Thereby, this way of calibrating the model is not convenient and not reproducible for other geometries without measurements. A positive aspect of this exercise is the conclusion that small deviations of roughness values are of very little influence on the flow field.

3.3.3 Laminar viscosity

The laminar viscosity is of influence on the turbulence modelling. The turbulence is modelled as a viscosity value. When increasing the value of laminar viscosity, the fluid in the model becomes more viscous. This can also be seen as an imposed value of minimal turbulence. This increases the model tendency to flow more viscous and therefore laminar in an earlier stage. It must be said that changing the value of molecular viscosity is not physically correct. This fluid property is well known and not a part of any discussion of modelling turbulent flows.

The influence of imposing a value of minimal turbulence is not very great (Figure 16 and Figure 17). A calculation with a molecular viscosity of 10^{-5} m^2/s, has a very comparable flow field as with the molecular viscosity (10^{-6} m^2/s). The main difference is in the velocity distribution of the flow under the ship. Here the figures show that the increased viscosity, results in more friction at this confined location. Calculations made with a further increased laminar viscosity, showed that the flow becomes laminar quickly after leaving the bowthruster.

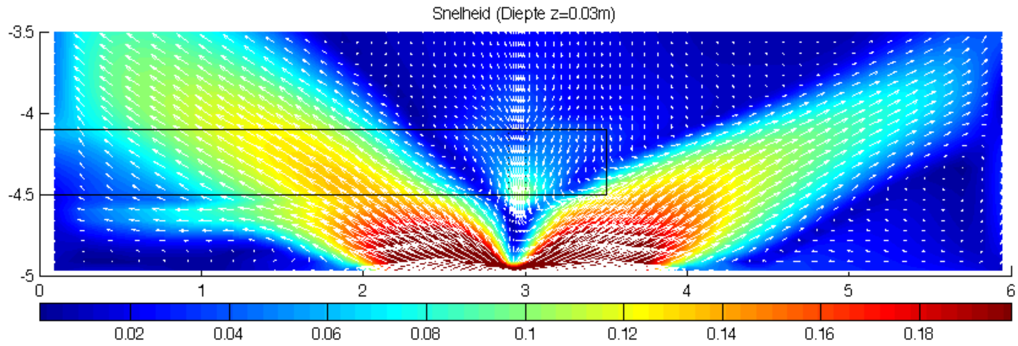

Figure 16: Flow field with a molecular viscosity of 10^{-6} m^2/s (standard case) on z = 0.03 m

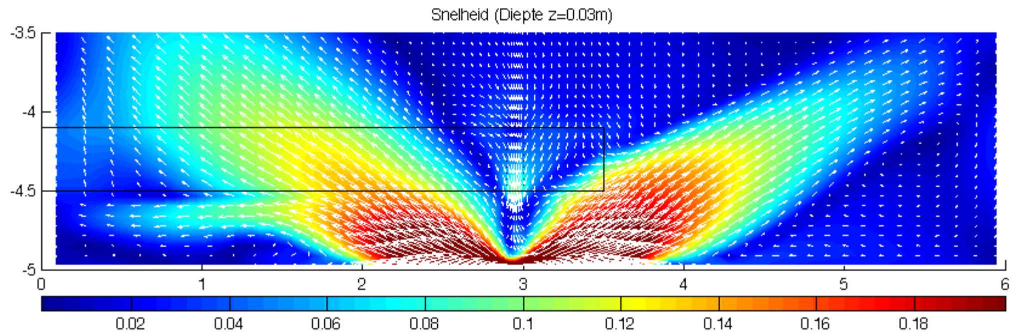

Figure 17: Flow field with a molecular viscosity of 10^{-5} m^2/s on z = 0.03 m

From these calculations, the conditions in the numerical model are highly turbulent. The flow becomes laminar only after increasing the value of laminar viscosity considerable. Basically, the threshold for the flow to behave laminar is not reached in the model. This argues in favour of the assumption of high turbulent flow and the use of the kε-turbulence model. As said earlier, changing the value of the molecular viscosity is not physically correct. Molecular viscosity is a property of the fluid.

3.3.4 Increasing the flow rate

To retain a similar level of the turbulence in the screw-pipe, the velocity should be increased with the same proportion the size is decreased (see formula 3.2). This is called Reynolds scaling. However, there is a physical limit to increasing the velocities. The water pressure before the screw is a limiting factor on the velocity it can produce. If the pressure before the screw drops to a negative value, cavitation will occur. Cavitation is the creation of gas bubbles due to under pressure in a fluid. These bubbles will implode when the pressure increases. These implosions can damage the screw in the model and a further increase of the velocity beyond this limit is not possible. With an ideal screw, it is possible to use all the water pressure to create a flow velocity. However, the ideal screw does not exist. So, using the pressure, only an upper boundary of the maximal flow velocity through the screw can be calculated. This maximum velocity will be calculated with zero water pressure on the upper side of the screw. This results in the following adapted formula of the Bernoulli equation for energy conservation:

$$u_{0;\max;ideal} = \sqrt{2g \cdot \left(d_{bs} + \frac{P_{atm}}{\rho g} \right)} \qquad (3.18)$$

where:

$u_{0;\max;ideal}$	= Maximal velocity for an ideal screw [m/s]
g	= Constant of gravitation [m/s^2]
d_{bs}	= Depth of the upper side of the screw below the water surface [m]
P_{atm}	= Air pressure on the water level (10^{-5}) [Pa]
ρ	= Density of water (1000) [kg/m^3]

For the different screw diameters, the maximum velocity that will be possible in the geometry of the physical model will be as shown below:

Screw diameter [mm]	d_{bs} [m]	$u_{0;max;ideaal}$ [m/s]
100	0,37	14,264
160	0,34	14,243
200	0,32	14,229

Because the ideal screw does not exist, the maximum value of the screw velocity in this geometry will be lower. Higher values are possible, but changes must then be made to the inflow to prevent cavitation. Narrowing the outflow after the propeller is a possibility. However, this will extensively influence the characteristics of the thruster.

In the calculations, increasing the flow rate through the bowthruster is not expected to be of any influence on the relative flow field. Besides some wall effects, the velocity-field and turbulence production are relative to the average axial screw velocity. Calculations of higher velocity situations confirmed this statement. Here is assumed that the turbulence energy level does not drop too far, to prevent the flow from to becoming laminar.

3.4 Influences of geometrical changes

Besides all the changes of flow properties, geometrical changes can also be of great influence. The geometrically changed calculations were made, to assess the influence of the chosen geometry on the flow field. There was a fear that the influences of the scaling the geometry was negative on the turbulence. The estimated Re-values are low (see par. 3.2). With changes in the geometry, the Re-values can be influenced.

Increasing the keel clearance

To see the influence of the restriction of the space under the ship, a calculation with a larger bottom clearance was made. In the description of the flow in the numerical model, the reflecting flow is bounded to the bottom and the water surface. The larger keel clearance gives more space for the flow on the harbour bottom. The reflecting flow becomes, for this reason, more symmetrical on the bottom. The ship is not able to damp the velocities on the bottom.

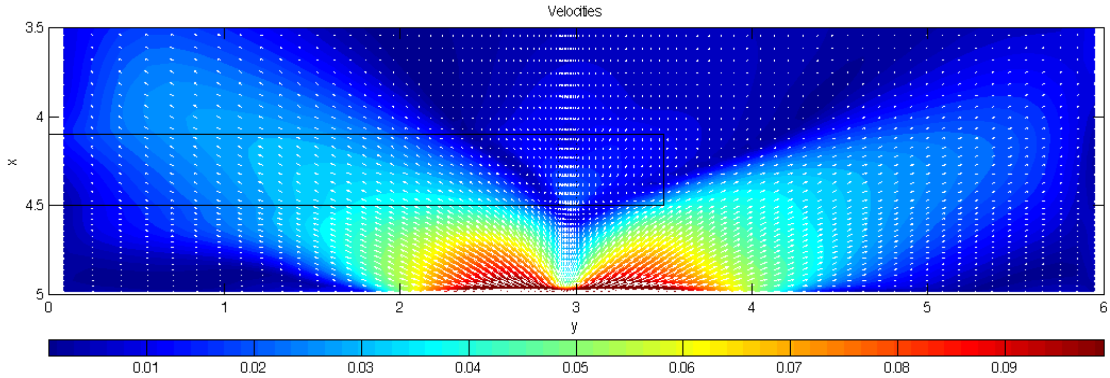

Figure 18: Flow field with a keel clearance of 0.10 m on z = 0.03 m

Lowering the water level

Lowering the water level has as consequence of a reduction in the flow area for a return flow. The area between the ship and the quay wall becomes less when the height decreases. This forces the flow to flow faster on other locations. Clearly visible is the re-orientation of the reflecting flow. The angle of reflection is far more reduced than in the original calculations. Strange however is the different location on the y-axis of the maximum velocity along the distance of the wall. The maximum velocity was at the reflecting current, and is now under the bowthruster. Here the suction of the bowthruster pulls a current. This current has much less turbulence as the reflected flow from the quay-wall. In addition, the velocities do not reach as far as from the quay-wall as in the original calculations. The change in space for the vortices around the swirling jet of the bowthruster resulted in a different flow field.

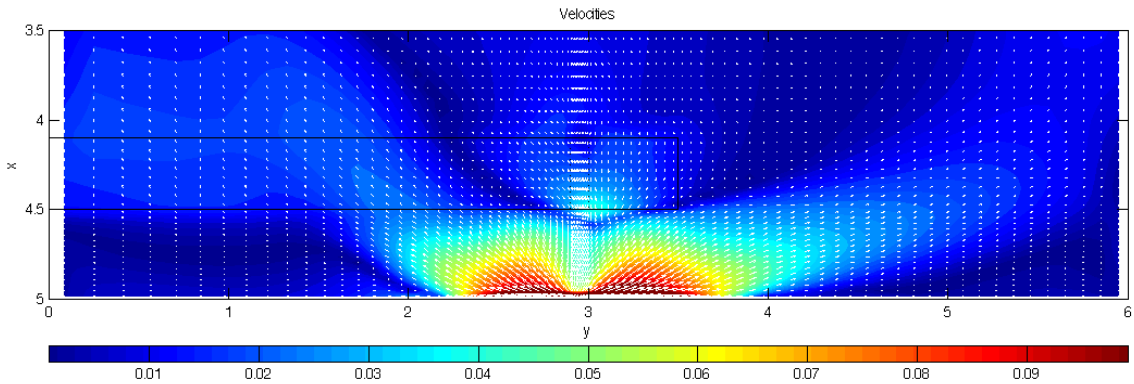

Figure 19: Flow field with a 0.20 m decreased water level on z = 0.03 m

Increasing the screw diameter

One of the possibilities to increase the flow velocities in the physical model is by increasing the size of the bowthruster. This has a very small effect on the cavitation limit of the screw. A recalculation shows that the flow field is changed. The high velocities are more concentrated along the quay-wall. This could be a result of the change in space for the vortices around the jet.

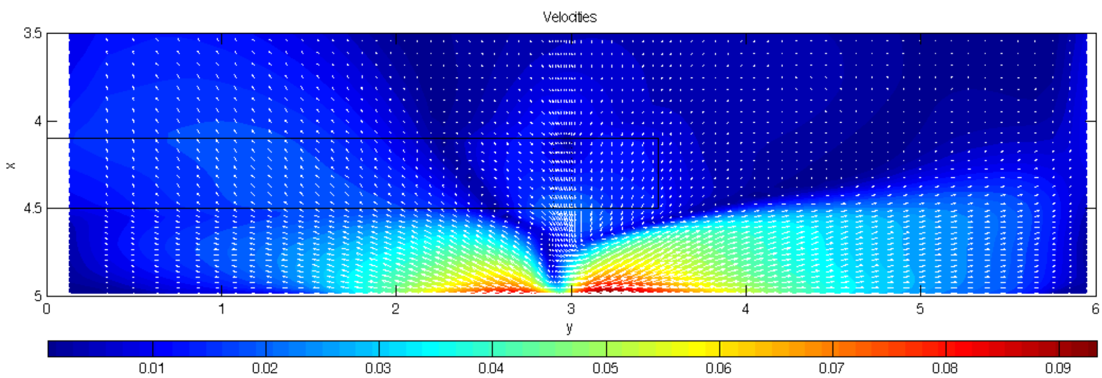

Figure 20: Flow field with a bowthruster diameter of 0.160 m on z = 0.03 m

3.5 Summary of the sensitivity analysis

When all results are summarised, it shows that the numerical model is insensitive to changes of the wall friction, molecular viscosity and a change of turbulence model. It is sensitive to geometrical changes. A summary is made in the table below.

Parameter	***Remarks***
turbulence model	The change of turbulence model is of very little influence of the results of the numerical model. The use of the kε-model, to model the turbulence seems justified. There could still be a difference with the physical model, due to the assumption of isotropic turbulence. The used turbulence models for comparison, all have this assumption.
wall friction	Different roughness values on the harbour bottom, quay-wall and ship, have very little influence on the flow velocities near to the quay-wall.
molecular viscosity	Changing the molecular viscosity is physically not allowed. This value is a property of the fluid. However, the turbulence is modelled as a viscosity. So increasing the value of the viscosity can also be explained as an assumption of a minimum value of turbulence in the numerical model. Increasing the value of the molecular viscosity has very little influence on the velocity distribution.
bowthruster flow rate	Increasing the bowthruster flow rate has no influence in the velocity distribution. The velocities in the flow field scale all with the same number as the average axial velocity in the bowthruster.
Geometrical parameters	
keel clearance	The keel clearance has a large influence on the velocity distribution on the bottom. Larger keel clearance results in a more symmetrical flow distribution on the bottom. The reflecting flow from the quay-wall is bounded to the harbour bottom. The keel clearance becomes less important on the flow distribution as the value increases.
water depth	The lowering of the water surface had a large effect on the distribution of the flow velocities. The maximum velocities are closer quay-wall. The change is a result of the change in space for the secondary flow to develop vortices around the water jet from the propeller.
bowthruster diameter	The change of the geometry of the bowthruster results in a large change of the flow field. The area for secondary flows to develop vortices around the water jet op the propeller did not change extensively, however, the velocity distribution on the bottom did. Where the flow reflected on the quay-wall in the original calculations, it now has a tendency to flow along the quay-wall.

For correct modelling of the bowthruster induced flows in a numerical model, it is important to model the outflow of the bowthruster correctly. This seems to be the most important aspect of the numerical model.

Chapter 4: Physical model

This chapter describes the physical model build by Van der Laan. The dimensions of the model are given in chapter 2. The factors of influence on the flow conditions are investigated here. They give a good estimate of the similarities of the physical model with the prototype flow. Finally, the instruments used for measurements in the model are reviewed.

4.1 Description of the bowthruster

The propeller in the bowthruster was earlier used in the model of Veldhoven and Schokking. The screw is a type of model screw used for hobby models of ships. The screw is not an exact scaled replica of a real screw for ships. The measurements of Veldhoven and Schokking, however, show a normal behaviour of the screw. The measurements of Schokking especially showed the collapse of the low velocity core, after some distance from the propeller. This was measured for a ducted and a free propeller.

De Jong, concluded from the measurements of Schokking that the ratio between the average axial screw velocity and the rotating screw velocity of the flow needed to be 0.8. De Jong called this ratio the swirl ratio. Later, the measurement will confirm the value of this ratio, when the outflow of the bowthruster is measured.

By trial and error, De Jong (2003) determined that the size of the core in the screw in the numerical model should be 30% of the diameter of the thruster. This was done for a screw in the middle of a thruster pipe of 0.30 m length. He derived this from the measurements of Veldhoven en Schokking.

Nielsen (2005) measured the flow-situation of one value for the axial velocity of the screw. The used rotation speed of the electric motor was 850 rpm. According to Van der Laan, this gives an axial velocity of the screw of 1.6 m/s. He calculated the average axial velocity in the screw from the measurements of Schokking and the gearing of the screw. Nielsen, however, reported this was 1.5 m/s. He did not describe the way the got his velocity. Possibly, he misread the report of Van der Laan. When the outflow was measured, both velocities were over estimations of the real averaged axial velocity of the screw in the physical model. This will be described in the next chapter.

4.2 Comparing the physical model to the real-life scale

The objective for building the physical model is to have a comparable flow situation to the real-life scale situation. If this is true, the model can be used for validating the numerical model. To assess the similarities, the scaling parameters for liquid flows are discussed. They are used to give an indication for the similarities of the flow situation in the physical model to the real-life scale.

Liquid flows have two scaling parameters. Both describe the scaling of different properties of the flow. It is impossible to scale from reality, and to hold both parameters at the same value, unless the model has the same dimensions as the prototype situation. However, these limitations are not a problem. For large deviations of the parameters, the properties of the fluid are the same. But, there are limits.

Froude

The Froude number gives an indication of the dynamic flow behaviour. The dynamical properties of the flows are given by this parameter. Flow situations, where the Froude number is important in the model have large slopes on the water surface, or changing flow conditions from sub-critical to super-critical flow. In most other situations, the value of the Froude number is less important. The Froude number can also be seen as a value for the influence of the gravitational energy on the flow.

Froude-number: $$Fr = \frac{U^2}{g \cdot l} \qquad \textbf{(4.1)}$$

Where:
Fr = Froude-number [-]
U = Flow velocity [m/s]
l = Length [m]

Reynolds

The Reynolds number gives a value for the turbulent conditions of the flow. The flow will become laminar when this value becomes to low. However, the minimum value of the Reynolds number is based on the assumption of the flow to be unstable and therefore flow turbulent. If the flow is turbulent upstream, it takes some time and distance to become laminar. The turbulence has to damp out.

The Reynolds number is give by:

$$\mathrm{Re} = \frac{u \cdot L}{\nu} \text{ [-]} \tag{4.2}$$

Where:

Re = Reynolds-number [-]
u = Flow velocity [m/s]
L = Length [m]
ν = molecular viscosity [m^2/s]

The flow velocity is the average flow velocity of the flow in the confined conditions. The length is a characteristic length of the flow situation. For the flow around an object, it is the width of the object. For flow through a confined space, it is the smallest available distance for the flow. The length for the flow under the ship is the keel clearance.

When the value of the Reynolds-number is low (below 3000), the flow is not capable any more to become turbulent. In these situations, the flow will be laminar. For decelerating flows, it takes some time and distance for a turbulent flow to become laminar. The turbulent energy needs to damp out. If the screw produces a high turbulent flow situation, the influences of the Low Reynolds numbers will only be noticeable far away from the screw.

To make a picture with the expected Re-values, a characteristic length must be found for every part of the model. For this length, the shortest length between the flow-restricting objects is chosen. This results in the lengths as they are visualised in Figure 21.

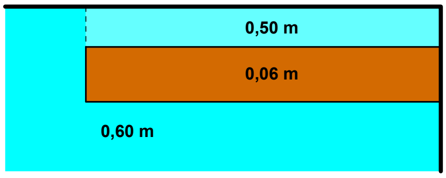

Figure 21: Length used for calculating the Reynolds-numbers in the models

De Jong (2003) already warned that the velocity underneath the ship could be too low. He suggested a minimum of 0.05 m/s to avoid problems related to low Reynolds numbers. This is based on Pearce (1996) recommendation of a minimal Reynolds-number of 3000 for fully turbulent flows. As it appears from the measurements and calculations, in some location under the ship, the velocities are too low. However, the value of Pearce is based on laminar flows, to become turbulent. The screw propeller is a turbulence source. The turbulence produced by this source is expected to be of a much higher energy level. It takes some time and distance for this energy level to damp out, before the flow becomes fully laminar. The low-Reynolds numbers will therefore not play a major role especially, in the region close behind the outflow of the bowthruster.

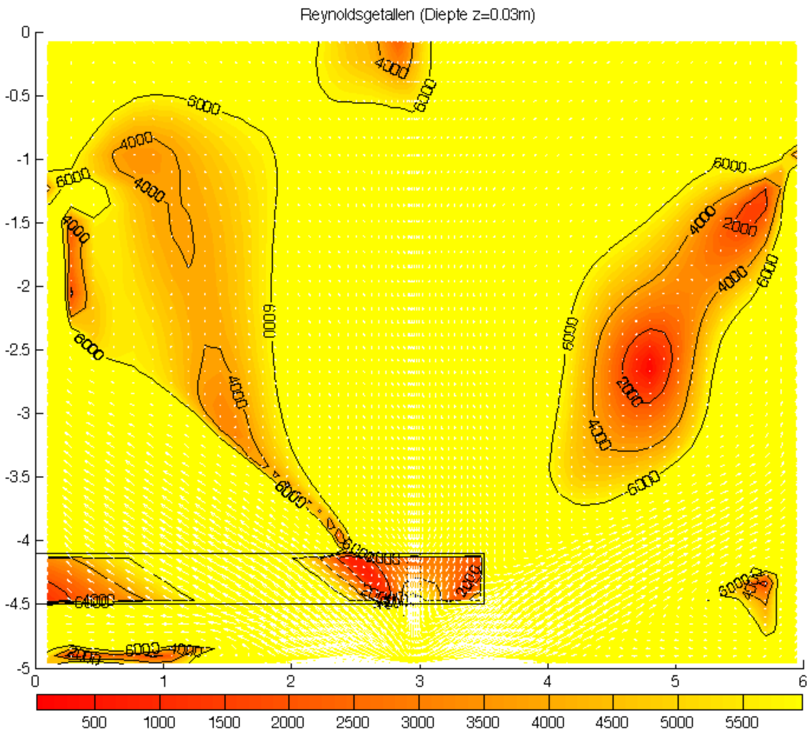

Figure 22: Reynolds numbers in the original calculation on z = 0.03 m

The figure above shows the Reynolds-numbers with the velocities calculated 0.03 m above the bottom. However, this is not the right characteristic velocity for the whole field; it is for underneath the ship. Only in the region under the bowthruster, where the flow is sucked with the jet-flow the turbulence will not be exerted by the screw propeller. At this location, a deviation of the numerical model from the measurements is expected. However, as stated before, calculations on prototype scale does not show any differences. Here the problem of the Re-values is non-existing due to the larger velocities and distances.

The same trick can be done with the measurements if the Reynolds-numbers are calculated from the measured velocity-field. This shows that the whole space under the ship is of low Reynolds-conditions (Figure 14). However, this is calculated with the measurements of Nielsen. As earlier stated, these are not accurate measurements.

4.3 Measurement instruments

To measure the velocities in the physical model, two types of instruments are used. Van der Laan and Nielsen used an EMS instrument. The measurements for this report were done with an ADV. The two types of instrument are describes, with there properties and faults.

EMS (Electromagnetic velocity meter)(link to Nielsen)

A description of the instrument is given in the appendix of Nielsen (2005). He and Van der Laan did measurements with an EMS instrument in the physical model. The EMS instrument measures the velocity of the flow, on the change of electromagnetic field. The instrument is due to the way it measures very sensitive for temperature changes.

The settings of the instrument determine the measurement accuracy. The accuracy is 1% of the measurement range of the instrument. The used setting for the instrument range was 1 m/s during the measurements of Nielsen. A size of 0.01 m/s of deviations of the instrument on the measured value can be expected. The most part of the measurements the measured values are of a size 0.01 - 0.10 m/s. A 10 - 100% inaccuracy on the measured value is very large.

The instrument is rather large compared to the geometry of the model. In the confined conditions under the ship, there is an influence of the instrument on the flow. The instrument was calibrated for the flow situation under the ship. However, these settings where used for all the measurement points.

The bottom has an influence on the measurement values. This was the main reason the instrument was calibrated especially for measurements in the physical model. This also restricted the use of the instrument to the calibrated situation. The measurements in front and to the side of the ship used the same settings of the instrument. The absence of the upper boundary could have a large influence on the velocity measurements.

ADV (Acoustic Doppler Velocimeter)

The measurements in this report are done with an ADV (Acoustic Doppler Velocimeter). A description of the instrument is in the appendix. The instrument has some advantages and disadvantages compared to the EMS instrument.

The main disadvantage is the needed seeding in the water. The EMS instrument measures in clear water, but the ADV needs non-water particles for a measurement signal. The water in the laboratory is generally too clear for any measurements with an ADV. The possibilities for this are in the appendix.

The ADV instrument has some advantages over the EMS. The first advantage is the capability of the ADV to measure a three dimensional velocity vector. With an EMS, it is only possible to measure a 2-D velocity vector. The presents of a third component influences the other two directions. Besides this, the size of the measurement volume of the ADV is smaller. It is also better defined as the volume for the EMS and here is no physical connection between the measurement device and the measurement point. This all is in favour of better and more accurate measurements.

Where the EMS blocks the flow, the orientation of the instrument can be changed to have an upstream measurement point of the instrument. This minimises the influence of the instrument on the flow measurements.

The influences of the walls on the measurements with an ADV are different as on the EMS. With the ADV, it was possible to measure closer to the walls. A minimal distance of 0.007 m was possible during the trial measurements in a flume. Of great influence on this distance was the orientation of the ADV. For this reason, it was decided to aim the ADV instrument at an angle to he measurements points. For all the measurement series, the z-axis was rotated with an angle of 45° to the z-axis of the physical model. When the results were processed, the different orientation of the instrument was corrected to the axis system of the physical model (see chapter 2).

To summarise the advantage and disadvantage of the ADV over the EMS, the table below is given.

EMS (See appendix Nielsen, 2005)	**ADV (See appendix A)**
Advantages: - The instrument can measure in clear water	Advantages: - Small measurements volume - Measurement of a three dimensional velocity vector - The influence of the instrument on the flow is minimal - Able to measure close to a wall
Disadvantages: - Unknown size of measurement volume - The instrument is a blocking object in the flow - It measures a 2-D velocity vector - Unable to measure close to a wall	Disadvantages: - The instrument needs seeding

Chapter 5: Measurements in the model

This chapter describes the measurements in the physical model. First, the choice of the measurement points of the four measurement series is explained. After this, the results are summarised and criticised.

In the physical model, several measurement series were done to get a better understanding of the properties of the flow field. From the calculations of chapter 2, it becomes clear that there are several differences between the numerical model and the measurements done by Nielsen (2005) in the physical model. In addition, an unexpected change in the calculated velocity field was noticed when the geometry of the bowthruster was changed. Based on the existing measurements and calculations of the model, several areas of interest are chosen. For these areas of interest, measurement grids are chosen and measured.

5.1 Choice of measurement grid

The formulas in the third chapter state that in the calculations, the value of the initial axial screw velocity is not important. All velocities scale with the same constant to the new situation. A minor influence is expected from the influences of the wall resistance. However, changing the wall-resistance in the calculations only had a very small effect. From all comparisons between calculations and measurements, it seems that the problem of modelling the flow of a ducted propeller flow is the modelling of the turbulence or the propeller. Measurements must be made to determine the flow field in this area so an assessment can be made of the needed changes on the models.

The measurements done by Nielsen were the starting point of this research. From the description of the original calculation, it became clear that some of the measured points should produce doubtful measurement results. The flow was in these locations not dominated with velocity components in the x-y plane. Because the measurement instrument could not cope with a vertical velocity component, this will have a disturbing effect on the measurement results of the EMS.

The first measurement series was done to control some measurements of the EMS (Nielsen). The decision was made not to redo all of the measurement points of Nielsen. A few points of the first measurement series and the EMS measurements were at the same location. These points are later used for comparing with the results of Nielsen in paragraph 6.3. The other points of the first measurement series were to assess another aspect of the flow in this location. The measurement grid with close measurements over the vertical gives some confidence over the measured values. Large differences in not expected regions can be a sign for faulty measurements. This measurement series also gives the opportunity to show the existence, of the region with 2-layer flow. In the numerical model, the layers have opposite flow directions over the vertical. A notification of this region in the physical model would be very interesting.

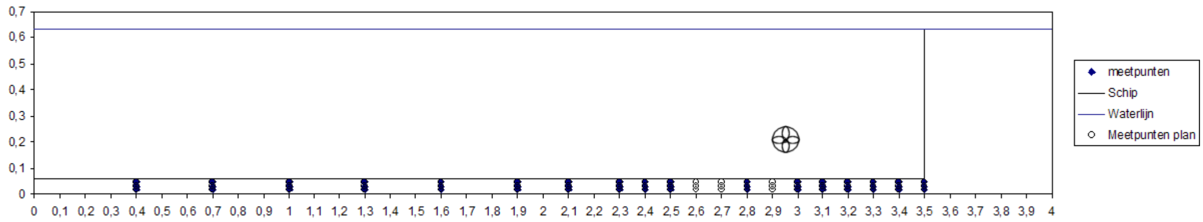

Figure 23: First measurement grid (cross section on x = 4.50 m)

The second and third measurements series are chosen to measure the propeller flow in the physical model between the quay wall and the ship. The third measurement series was extended to measure also some points at the inflow of the bowthruster. This was especially done to show the importance of the inflow. Hereby the gearing system to drive the screw is shown to be of very small influence.

If there is a modelling problem in the numerical model, it is most likely to have an origin in the source of the flow. In the second chapter, it was already noticed that a change of the propeller geometry have an extensive influence on the flow field. This while changing other variables has a much smaller impact. It is therefore important to know the behaviour of the flow field between the ship and the quay-wall. By measuring a vertical and horizontal velocity plane, it can also be assessed if the flow properties of the propeller in the physical model are the same as in the numerical model.

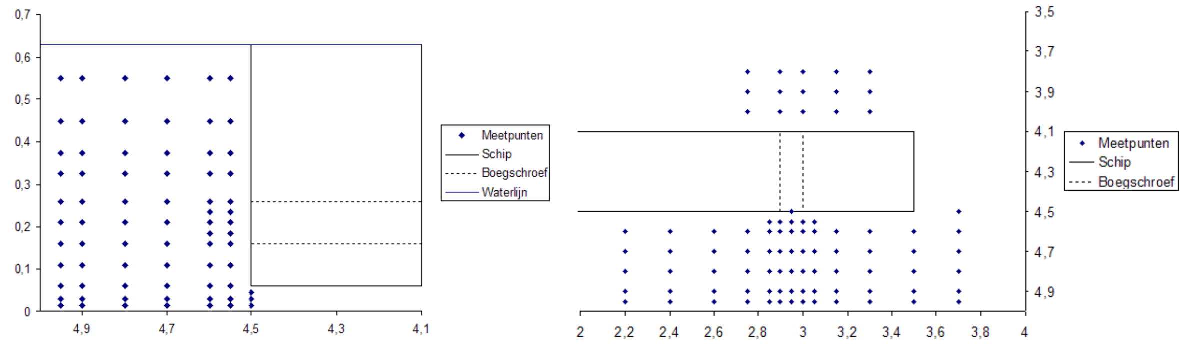

Figure 24: Second and third measurement grid (cross sections on y = 2.95 m and z = 0.21 m)

The fourth and last measurements series is done to determine the outflow of the bowthruster. This is a vertical line at a distance of 0.005 m from the outflow of the bowthruster in line with the screw axis. During the measurements of the second and third measurement series, the velocities produced by the bowthruster were lower as expected. Originally, the axial velocity of the bowthruster was calculated from the rotation of the electric motor. There could be a miscalculation with, for instance the geometry of the screw. In addition, the amount of turbulent energy needs to be checked. This is important for future stability calculations of the bottom protection. Most likely the turbulence in the physical model and the numerical model are not equal.

5.2 Results of the measurements on the edge of the quay wall side of the ship

The first measurement field gives the flow-situation under the edge of the quay-wall side of the ship. The regions of 2-layer flow with opposite flow directions, as was expected from the numerical model do not exist (see paragraph 2.2.1). This measurement partly confirms the measurements done with the EMS by Nielsen. The next logical step is to visualise what flow field the bowthruster produces.

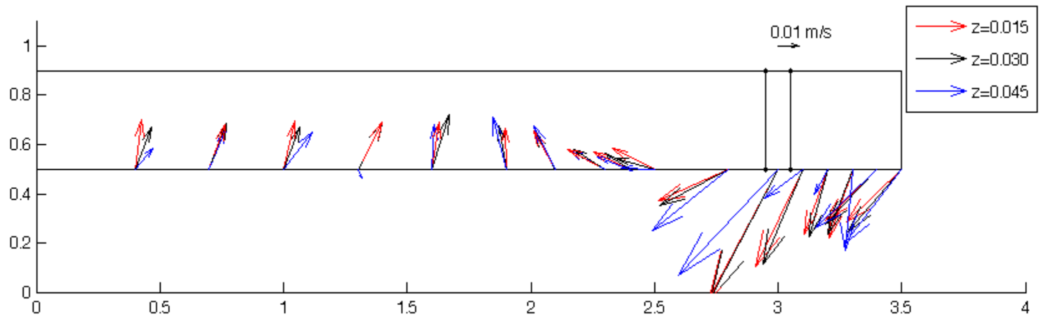

Figure 25: Results first measurement grid

(x-coordinates give the distance from the quay wall)

5.3 Measurements horizontally/vertically

The measured velocity-fields of the jet-flow is visualised in the figures below. They show the flow field of the bowthruster in the area between the ship and the quay-wall. The results are actually quite shocking. From literature, it is known that the core of a propeller flow collapses after distance of 2 or 3 times the diameter of the propeller. The measurements here show that this is not true for this case of bowthruster-induced flow. The core exists on the whole length from propeller to quay-wall. It grows in size and has a major contribution to the flow distribution. The quay-wall is situated 5 times the propeller diameter behind the outflow of the bowthruster. Veldhoven and Schokking used the same propeller for measurements of the flow situation on a slope. They noticed the collapse of the core in all measurements, within a distance of 3-5 times the diameter. This distance was shorter for the free propeller as for the ducted propeller. However, they did not measure a growth of the low-velocity core.

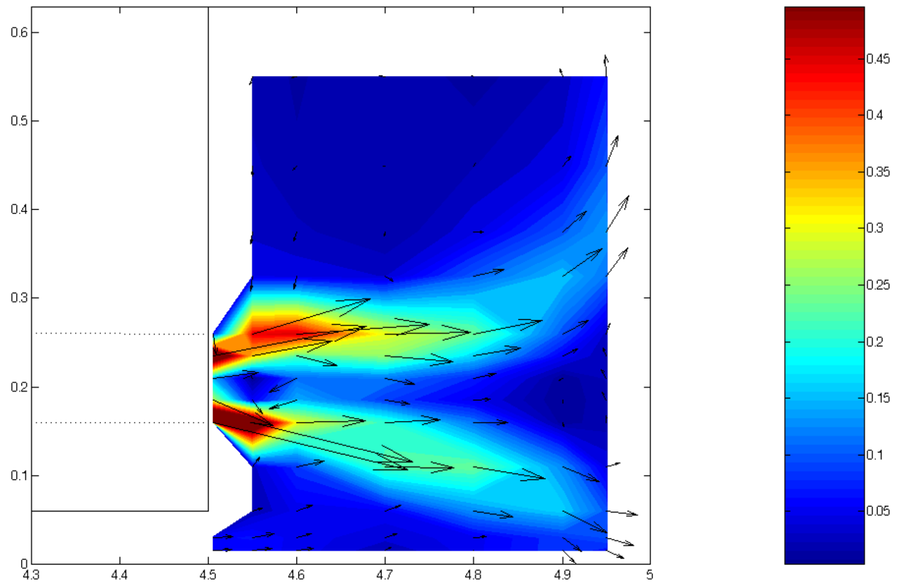

Figure 26: Measured cross-section of the vertical velocity field on y = 2.95 m

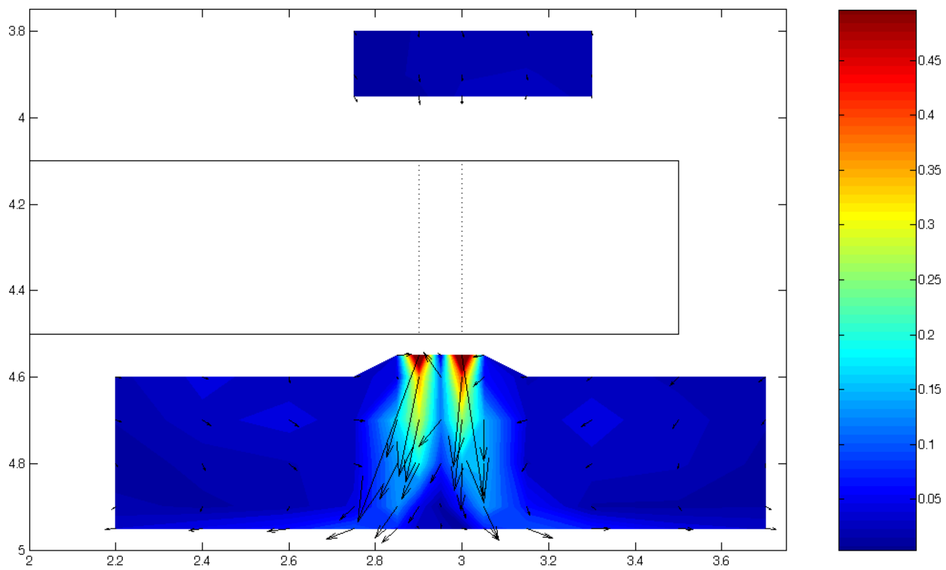

Figure 27: Measured cross-section of the horizontal velocity field on z = 0.21 m

5.4 Measurement of the flow rate of the screw propeller in the model

The calculations seemed to have larger velocities as the physical model especially at the outflow of the flow pipe. These differences are important for the comparison between the calculations and the measurements. Therefore, the outflow of the bowthruster is measured. The amount of turbulence produced with the propeller is not yet verified. A calculation with the right amount of turbulence on the bottom is not yet possible. The measurements on the outflow are done on a distance of 5 mm from the real outflow. The orientation of the instrument did not allow measuring the velocities any closer. The results of the measurements are given below.

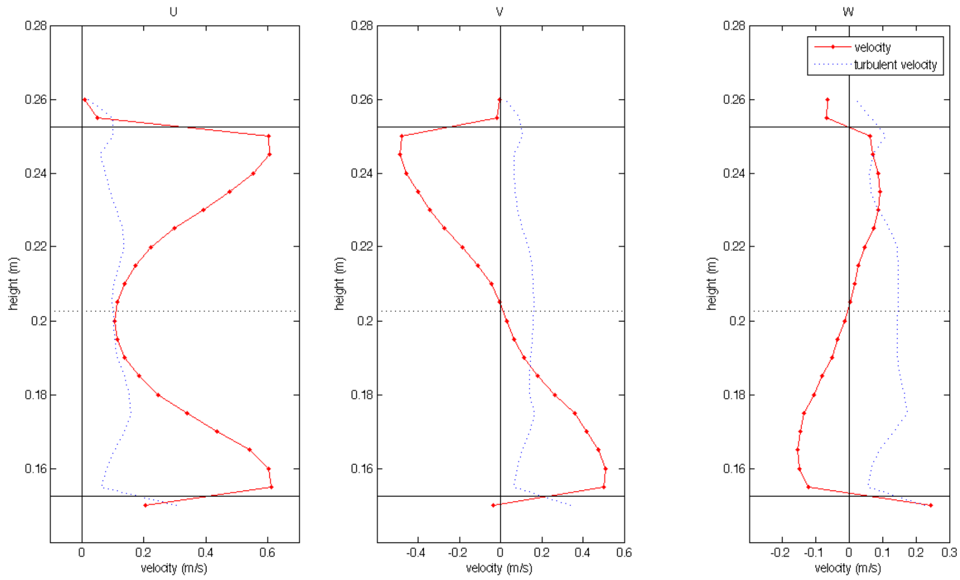

Figure 28: Velocity measurements on the outflow of the bowthruster (y = 2.95 m, x = 4.55 m)

The measurements give the expected results for velocity distribution close behind a propeller. The only problems are the distance of the measurements from the propeller and the value of the velocities. Expected was a mean velocity of 1.6 m/s (Van der Laan, 2005) with the used setting of 850rpm on the engine. This is an overestimation of the bowthruster velocity present in the model. The table of velocities made by Van der Laan (2005) could be miscalculated, or the assumed properties of the propeller were not correct. From the measured velocities an average flow rate can be assessed by integration over the area and the assumption the velocity field is axis symmetrical. This results in a flow rate of 0.0035 m3/s and an average axial velocity of 0.45 m/s. This value will be used for the calculations on modelling the bowthruster.

The turbulent stresses can also be calculated. However, the expectations are that the distributions of the absolute values of turbulent stresses would be axis-symmetrical. This is not the case. The differences could be the result of an influence of the walls on the measurement instrument. This influence must be small, other wise it would also have showed in the values of the mean velocities.

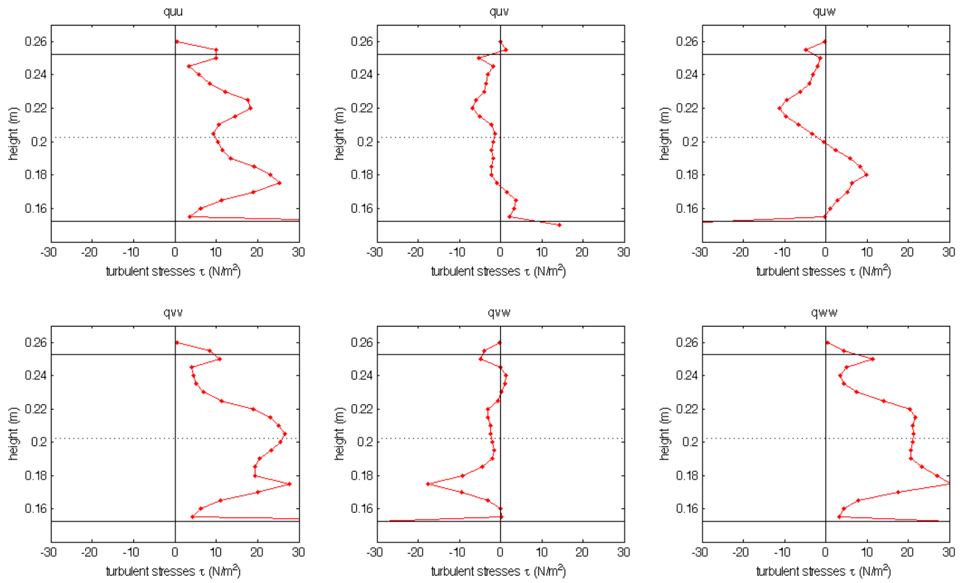

Figure 29: Turbulence measurements on the outflow of the bowthruster (y = 2.95 m, x = 4.55 m)

Chapter 6: Modelling the ducted propeller

In the previous chapter, the outflow of the bowthruster in the physical is measured. With these results, the bowthruster in the numerical model can be adapted to the situation of the physical model. After comparing the adapted calculations on the numerical model with the measurements in the physical model, a comparison is also made with the EMS measurements of Nielsen. The adapted numerical model is also used to calculate the velocity distribution on the bottom for two positions of the ship. These results are compared with the analytical models, described in chapter 2.

From the last measurement grid of the previous chapter, it shows that the velocity distribution of the outflow of the bowthruster is of an unexpected shape. This shape would be expected if the measurements were done very close to the propeller. The knowledge of a free propeller flow, tells us that the low-velocity core after the propeller collapses within a length of 2-3 times the diameter of the screw. This means that if the tube belongs to this distance, the core should faintly, or not exist at the measured distance from the outflow. The most likely explanation is that the flow pipe damps the tendency to redistribute the flow. In the analytical models, however, the collapse of the core is assumed to start from the outflow of the tube. The measured flow field in the second and third measurement grids shows this not to happen in the physical model. The low-velocity core exists from the outflow till the wall.

6.1 Modelling the jet-flow of a ducted propeller wash

The way of modelling the bowthruster could be important for the flow field it produces. Several calculations are made to assess which parameter should be altered to get a comparable flow field between the measurements and the calculations. The calculations below are all adapted to the flow velocity of the measured model. The measured flow rate in the bowthruster of 0.0035 m3/s is used as primary velocity source.

6.2 Original calculations with smaller calculation grid

In the original calculations, the ducted screw propeller flow does not give the same velocity distribution as is measured in the physical model at the outflow of the bowthruster. However, in the past the velocity distribution of the outflow was not expected to be of great importance. Until now, most measurements on propeller flows, showed the collapse of the low velocity core after some distance behind the propeller. Modelling this aspect of the propeller flow, would therefore not be necessary.

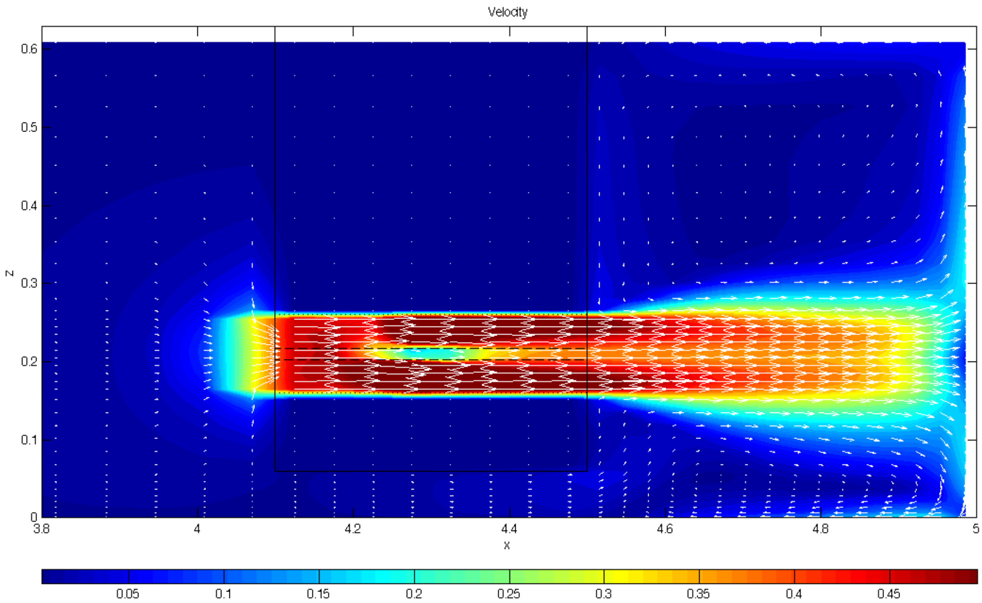

Figure 30: Original calculated velocity field on y = 2.95 m

The outflow of the bowthruster in the numerical model is similar to the analytical model of Schmidt. It is also very similar to the measurements of Schokking (2002), which were done on the same screw in a different geometry. However, these results are in contradiction with the measurements in the physical model. A low-velocity core should exist from the outflow to the wall. This feature could be the cause for the different results of the measurements and calculations. A way of modelling this aspect needs to be found. If it is done successfully, the validation for the numerical model can be done. Primary objective is to produce a similar outflow of the tube as is measured in the physical model.

6.3 Addition of plate at the inflow

To be certain that the differences between the measurements and the calculations are not the result of the not modelled restrictions of the inflow in the physical model, a calculation is made with the drive shaft and wheel in the model. The picture below shows that this does not makes any difference. The influence of the drive shaft is almost non-existing. This was expected, because the propeller eliminates almost all previous influences, when the water passes through.

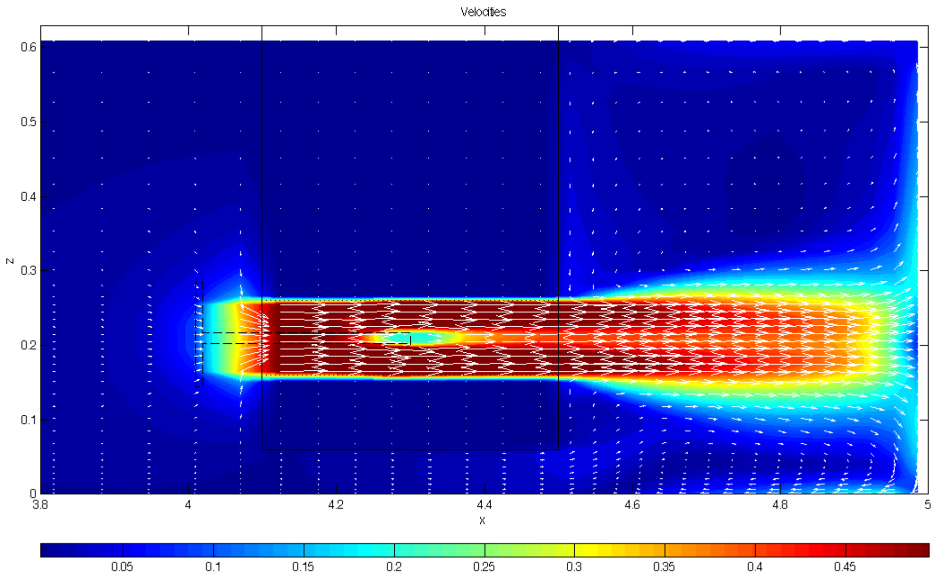

Figure 31: Calculated velocity field with the drive shaft and wheel on y = 2.95 m

6.4 Extending the screw axis over the whole width of the ship

It seems that the low-velocity core is not properly maintained to the outflow of the tube. For this reason, the axis centre is not of low-velocity conditions as is expected from the measurements. By extending a drive shaft along the whole width of the ship this low-velocity core can be forced. The result is shown below. However, the low-velocity core is present. The outflow still is not as measured. Notice needs to be taken to the length of existence of the low-velocity core. The propeller flow produces a core, which collapses at approximately 3 times the screw diameter (in Figure 31at x = 4.8 m). Here after, the fully developed velocity distribution of the analytical models appears.

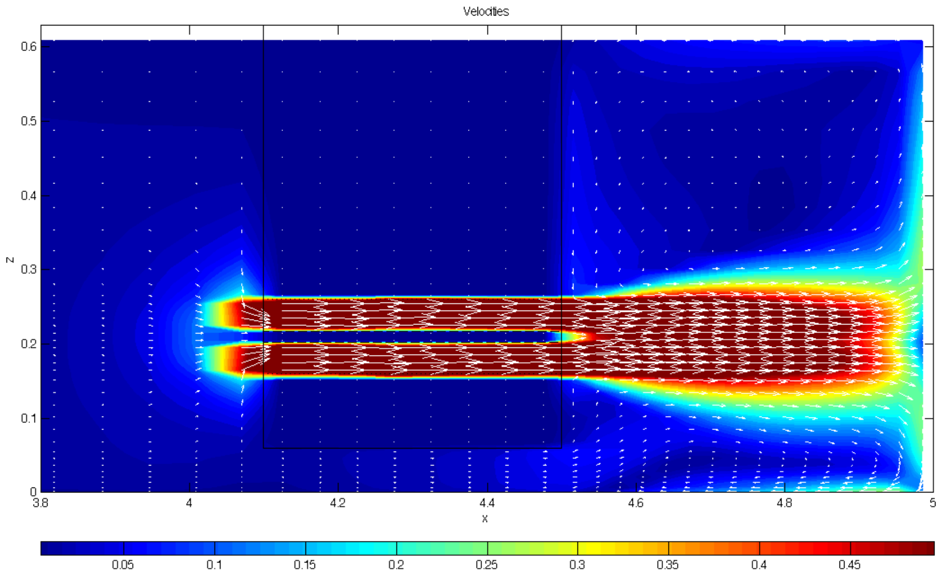

Figure 32: Calculated velocity field with a drive shaft over the whole width of the ship on 2.95 m

6.5 Enlargement of screw axis plate

From everything above, it seems that the velocity distribution produced with the propeller has the wrong shape. By enlarging the centre plate in the propeller, the source forces the velocities on a small area at the wall of the tube. When the velocities reach the outflow, diffusion will redistribute the velocities in the tube. The right size of the centre plate, should reproduce the velocity distribution of the measurements at the outflow of the bowthruster.

Enlarging the inner centre plate of the screw, works very well. The velocity distribution is similar to the measurements. The centre plate forces a very large low velocity core, which strangely shrinks and grows in the pipe. One of the probable causes for this to work could have an origin in the basics of a numerical model. The accuracy of the calculations is heavily dependent on the grid size. The calculations in the bowthruster are done with a very coarse grid. In the tube, numerical diffusion could play a vital role in the diffusion of the velocities. It could also have a cause in the level of turbulence the propeller produces in the numerical model and the velocity distribution of the propeller itself in the physical model.

A positive aspect is the rapid deceleration of the flow velocities after the outflow of the bowthruster. The large diffusion just after the outflow, results in a larger area for the flow. This aspect causes far lower velocities at the wall and the bottom.

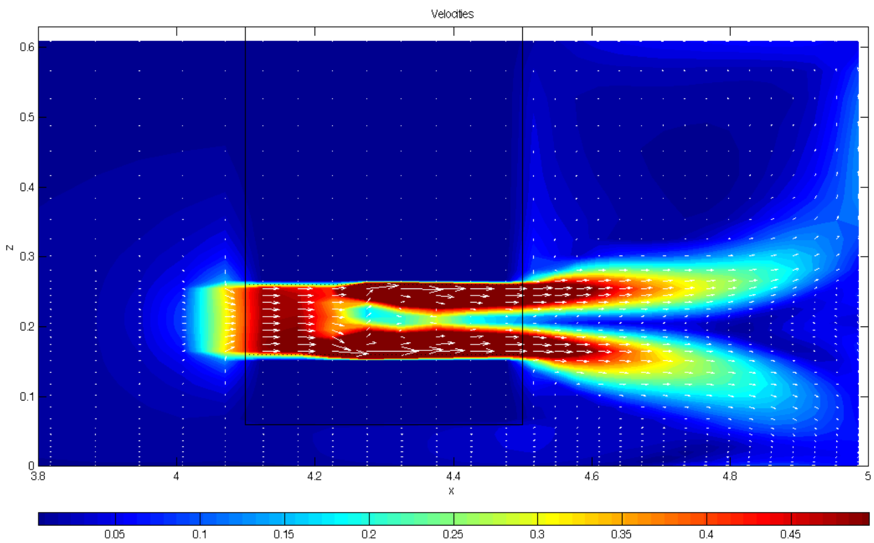

Figure 33: Calculated vertical velocity field with a centre plate of 0.085 m on y = 2.95 m

When we look at the flow field, the calculations of Figure 33 are very comparable to the measurements of Figure 26. But when we plot the calculated velocities in the measurements of Figure 28, the only deviating values are the vertical velocity and the turbulence (see figure below). That the numerical model produces to less turbulence is easily repairable by adding a turbulence source in the screw. For now, a factor of 3.5 solves the problem of the magnitude at the outflow. The shape of the turbulent distribution is strange for the measurements. This could have several causes. At first the distance and orientation to the wall of the measurement instrument could play a role. In this case, deviations on the measured average velocities are also expected but a few velocity peaks in the measurement signal will have a large impact on the turbulence and a minor impact on the average velocity. The frequency of the turbulent fluctuations could also have caused the deviations. Fluctuations within the time used for measuring the velocities, are averaged. This part of present turbulent energy will not be measured.

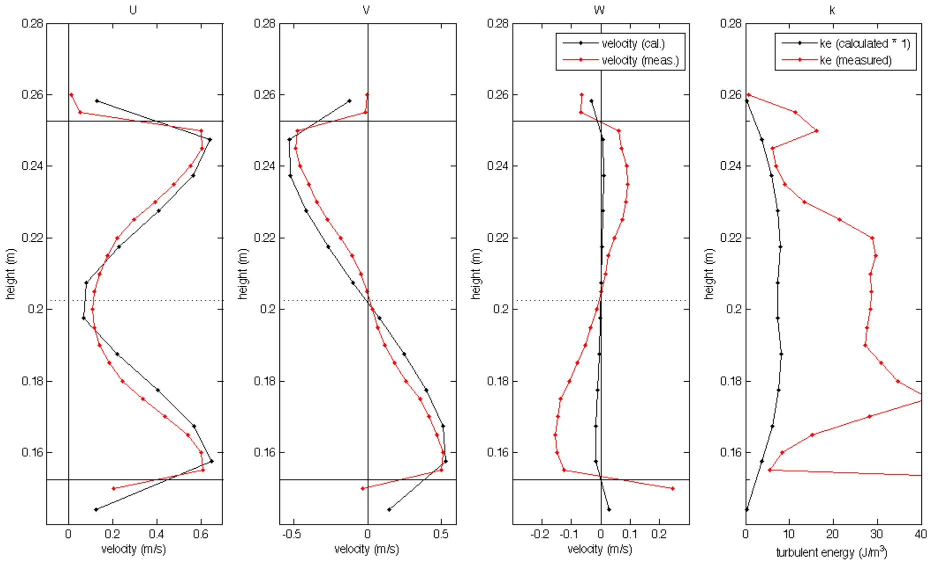

Figure 34: Comparison between the calculated and measured velocities (y = 2.95 m, x = 4.55 m)

The vertical velocities of the outflow in the calculations are to low. This could be a result of the chosen numerical grid. The values are interpolations between the points where they were calculated. If the vertical velocities rapidly increase and decrease at the outflow, this cannot be shown in the calculations. However, the vertical velocities are not the same. The diffusion of the propeller wash is approximately equal to the measurements. This is a strong indication that the differences in vertical velocities are cause by a lag of resolution.

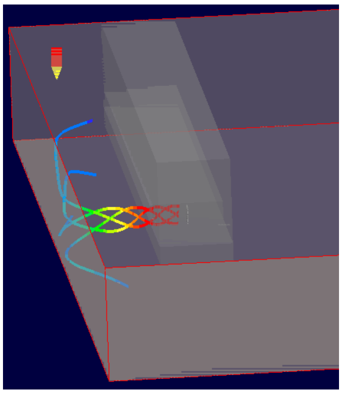

Figure 35: Streamlines from the bowthruster visualise the swirling motion of the jet-flow

The presents of a large low velocity core from the outflow of the bowthruster till the quay-wall, remains strange. One of the possible explanations is the presents of a higher pressure in the core. This would be a wedge in the swirling outflow of the bowthruster. However, a pressure plot of the calculations reveals that in the numerical model a wedge with higher pressure is not present. The pressure is the highest on the locations where the swirling water jet hits the quay-wall. A lower pressure on the height of the thruster axis at the quay-wall confirms the situation of the flow field. The swirling flow has the highest velocities in a ring that is growing in size from the outflow till the wall. This means that at the wall the velocities hit is at an angle. The highest pressures on the wall are at the location where the ring with high flow velocities make there impact. Because the flow is directed outwards from the axis centre, a lower pressure will be found on projection point of the axis centre on the wall.

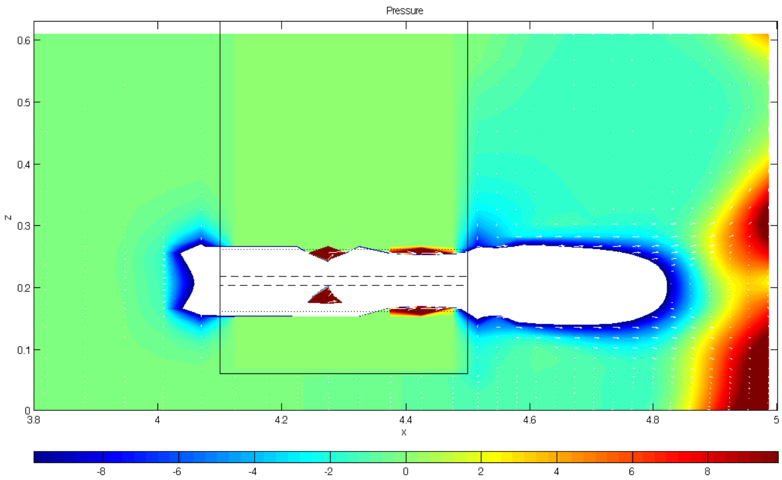

Figure 36: Pressure of the adapted numerical calculation on y = 2.95 m

There is another possible cause for the presents of the core. The centrifugal forces of the propeller-wash could cause the swirling flow to expend outwards, just after the outflow. This seems, for now, the best explanation. It also does not contradict with the difference in vertical motion between the outflow of the calculations and the measurements. The grid of the calculations is too coarse to show this. The anomalies in the pressure distribution at the outflow (Figure 36), suggest the presence of an anomaly. It is probably correctly modelled, but not clearly visible, because the resolution of the calculations is to low at this location. However, the adaptations on the bowthruster were not done on the rotational character of the propeller. If this suggestion is true, the size of the core has an influence on the rotational forces.

The modelling of the turbulence has large deviation from the physical model. Figure 34 shows that the amount of turbulence from the outflow of the bowthruster in the numerical model is far lower as measured in the physical model. The distribution of the turbulence is also different. The measured turbulence in the outflow of the bowthruster is not axis symmetrical. For this reason, there are some doubts on the measured values. Possibly, the scale of the turbulent fluctuations is in some measurement points to small to be measured with the used instrument and settings.

When the turbulence in the propeller of the numerical model is increased (an addition of a turbulence source), this will effect the turbulence on the outer circle of the bowthruster. The deviations on turbulence distribution (Figure 37 and Figure 38) between the quay-wall and the ship will probably become less. At this moment, the turbulence in the numerical model is mainly produced and maintained in the regions with large velocity differences. For instance, the region between the low-velocity core and the high velocity outer swirl of the propeller flow field. Only on the bottom, the turbulence seems comparable. However, the turbulent distribution is different in the calculations from the measurements. This could be a lucky strike.

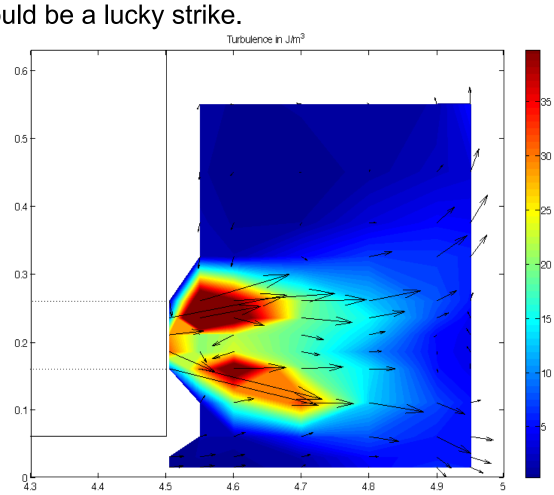

Figure 37: Measured turbulent energy on y = 2.95 m

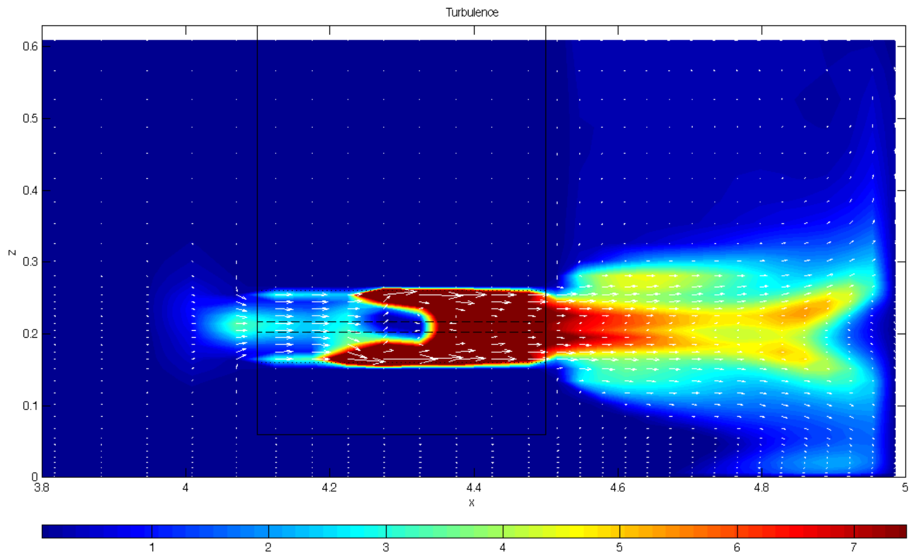

Figure 38: Calculated turbulent energy of the adapted bowthruster on y = 2.95 m

6.6 Comparisons of measurements

For a few measurement points, there are measurements of the EMS and the ADV. When put in a table, the differences between the results are shown. Although, there are large deviations in the magnitude of the velocity vector they all give similar results. Even when compared to the results of the adapted numerical calculations. All the values are within a 60% difference on the ADV measurements if these measurements are taken to be the real velocities in the model (is not assumed being true). The EMS gives generally an over estimation of the velocities. This was expected from the confined conditions. The instrument blocks the flow partly and therefore the velocities increase under the EMS, where it measures. The numerical model gives generally an under estimation of the velocities. This could be the result of the large value (0.001 m) of wall roughness in the numerical model, compared to the physical model. Some low-turbulence flow in the physical model could also have played a role.

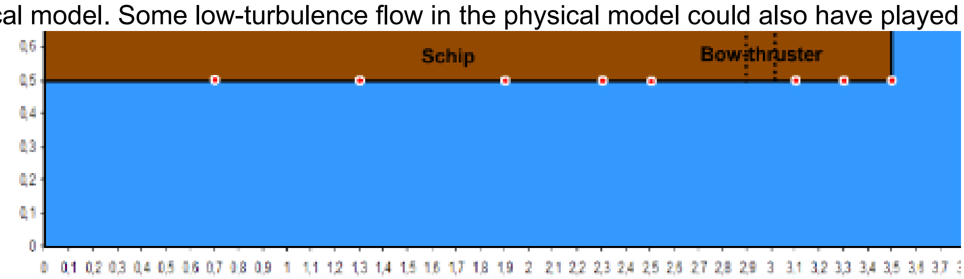

Figure 39: Location of comprison points on z = 0.03 m

x	y	z	ADV measurements	EMS measurements (Nielsen)	Numerical model	Difference	
m	m	m	m/s	m/s	m/s	ADV - EMS	ADV – Numerical model
4.50	0.70	0.03	0.026	0.029	0.025	-12%	4%
4.50	1.30	0.03	0.032	0.032	0.028	0%	12%
4.50	1.90	0.03	0.021	0.029	0.022	-38%	-6%
4.50	2.30	0.03	0.027	0.018	0.013	33%	52%
4.50	2.50	0.03	0.020	0.022	0.009	-10%	53%
4.50	3.10	0.03	0.050	0.069	0.036	-38%	28%
4.50	3.30	0.03	0.033	0.051	0.029	-55%	12%
4.50	3.50	0.03	0.040	0.051	0.028	-28%	29%

6.7 Comparison with the analytical models

After establishing the possibility to calculate the velocities produced in the model, it becomes interesting how it compares to the already existing models. When a plot is made of the maximum velocities at different heights, the velocity distributions on the bottom is shown. The different heights are plotted, to show if there is a large velocity distribution. This could be important for stone stability calculations.

When we make the velocities relative to the initial axial velocities of the screw, they are easily comparable to the analytical models of Schmidt and Blokland. An additional calculation of another situation can show some differences on the models. The first comparison is the situation as it was in the physical model. For the second comparison, the distance between the quay wall and the ship was reduced to ¼ of the length of the bowthruster tunnel. This was done with the same model for the bowthruster. This and other situations still need to be validated, but the results are already interesting. It shows the differences between the analytical models and the possible application of the numerical model.

Comparison on the geometry of the physical model

Model	**Relative velocity (%)**
Blokland	39.4 %
Schmidt	34.3 %
Numerical calculations	35 %

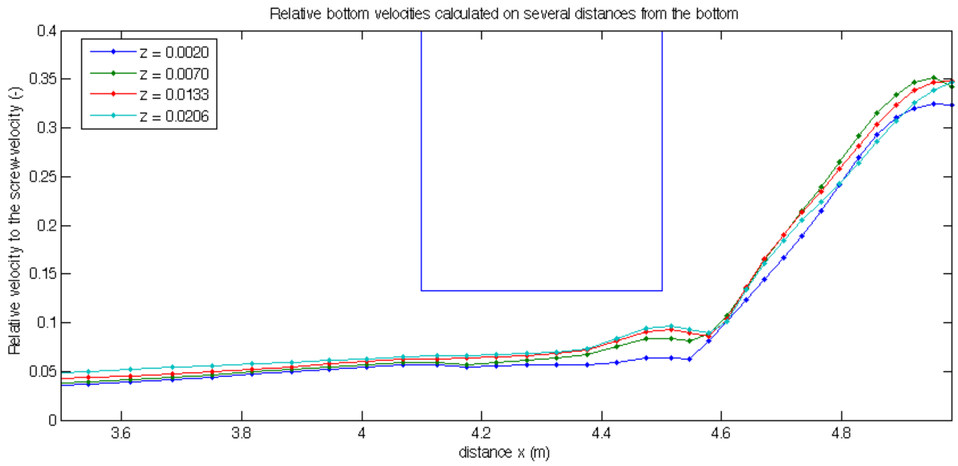

Figure 40: Maximum bottom velocities in the geometry of the measurements

Comparison with a distance of the ship to the quay wall changed to ¼ the length of the bowthruster

Model	**Relative velocity (%)**
Blokland	47.6 %
Schmidt	100 %
Numerical calculations	57 %

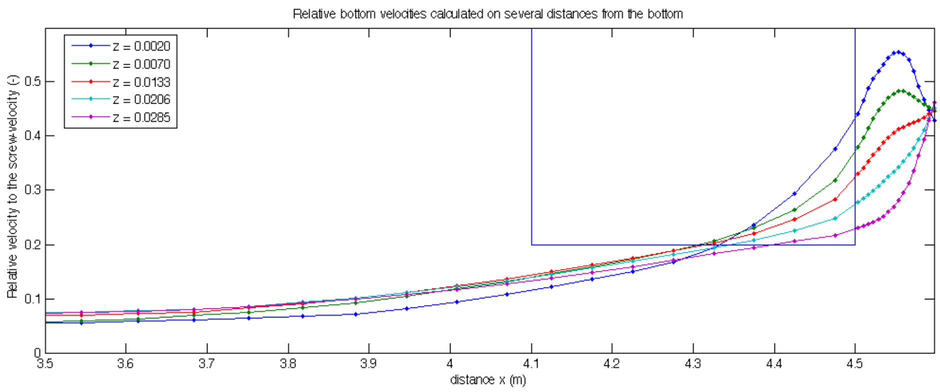

Figure 41: Maximum bottom velocities of a ship close to the wall

Chapter 7: Recommendations and Conclusions

7.1 Conclusions

A numerical CFD (Computational Fluid Dynamics) -model with a kε-turbulence model can be used for modelling the bowthruster-induced flow. However, the bowthruster must be modelled with great care. When the outflow of the thruster in the numerical model does not approach the outflow of the thruster in reality, there will be large deviation between the model and reality. The properties of the thruster are of great influence of the generated flow field.

The analytical models predict the collapse of the low-velocity core within a distance of 2.0 - 3.0 times the diameter of the thruster. Measurements in the physical model contradict this. The low-velocity core is present from the outflow of the thruster till the quay-wall. The core probably exists due to the centrifugal forces of the rotating flow. A higher pressure within the core could also have generated it, but the calculations do not show this. The presents of the core have implications for the validity of the analytical models. Their physical background and assumptions are doubtful.

To have a similar outflow of the bowthruster in the numerical model as in the physical model, the thruster needs to be modelled as a propeller with a centre plate. The diameter of the centre plate is 0.085 m in a thruster with a diameter of 0.10 m. This is only valid for the used propeller. Other types of screws can give different values. It would be better to define the real outflow velocities of the thruster in the numerical model, with associating values for turbulent energy.

The numerical model is insensitive for deviation of roughness of the different elements. Small changes of wall resistance are of almost no influence. However, changes in the geometry result in changes of the flow field, especially on the geometry of the bowthruster.

The turbulent energy level of the numerical model is far lower as measured in the physical model. The addition of a turbulence source, in the bowthruster of the numerical model, will solve this problem.

The measured velocity of the physical model was lower as assumed in the reports of Van der Laan (2005) and Nielsen (2005). Van der Laan reported the axial velocity to be 1.6 m/s with an 850 rpm of the motor. He derived this from typical characteristics of a propeller and the used gearing in the physical model. Nielsen reported that this should be 1.5 m/s. Integration of the measurements in this report give an average axial velocity of 0.45 m/s.

7.2 Recommendations

To assess the influence of the type of screw and the implications for modelling the thruster, some different types of screws or water jets need to be tested. Measurements of these tests will show the difference in the physical model. Low velocities and different screw types in the physical model can result in different flow conditions. In the current physical model, most turbulence is produced in the bowthruster. When the velocities become to low, the low-Reynolds numbers become important.

When different positions of the ship are measured and calculated in the current models, the range of validity of the numerical model becomes clear. The measurements do not need to be very extensive. When the velocities at some characteristic points are measured, the models can be compared.

The measurements on the flow field behind the bowthruster revealed a low-velocity core from the thruster to the quay wall. Other measurements and the analytical models predict a collapse of the core after 2.0 - 3.0 times the diameter of the screw. Some more situations need to be measured to establish the conditions for the core to exist beyond this distance.

References

Blokland, T. and Smedes, R.H. *In situ tests of current velocities and stone movements caused by a propeller jet against a vertical quay wall*, Gemeentewerken Rotterdam, 1994

Blokland, T., Smedes, R.H. *In situ tests of current velocities ands stone movements caused by a propeller jet against a vertical quay wall*, Rotterdam public works, Harbour Engineering Division, 1996

Jayatilleke,C.L.V. *The influence of the Prandtl number and surface roughness on the resistance of the sublayer to momentum and heat transfer*, Prog. in Heat & Mass Transfer, Vol.1, Pergamon Press, 1969

Jong, M. de, Het ontwikkelen van een model voor boegschroefstralen bij verticale kademuren, Master Thesis, Delft University of Technology, 2003

Laan, T. van der, *Het ontwikkelen van een model voor boegschroefstralen bij verticale kademuren*, Delft University of technology, Master Thesis, February 2005

Launder, B.E. and Spalding, D.B. *The numerical computation of turbulent flow*, Comp. Meth. in Appl. Mech. & Engng., Vol.3, p269, 1974

Nielsen, B. (2005) Bowthruster induced damage, Delft University of technology, Master Thesis

PIANC *Guidelines for the design of armoured slopes under open piled quay walls*, Supplement of PIANC Bulletin 96, Brussel, 1997

Sasaki, T., Nagai, N., Murai, Y. and Yamamoto F. *Particle Image Velocimetry measurement of bubbly flow induced by alkaline water electrolysis*, Proceedings of PSFVIP-4, June 3-5, 2003, Chamonix, France, F4007, 2003

Schmidt, E., *Ausbreitungsverhalten und Erosionswirkung eines Bugpropellerstrahles vor einer Kaiwand*, Leightweiss-Institut für Wasserbau der Technischen Universität Braunschweig, Mitteilungen, Heft 143/1998

Schokking, L.A. *Bowthruster-induced Damage*, Delft University of technology, Master Thesis, June 2002

Veldhoven, V.J.C.G.L. van, *Vooronderzoek schroefstraal op een talud met breuksteen, stroomsnelheden en steenstabiliteit*, Delft University of technology, Master Thesis, January 2002

Wilcox, D. C. (1994) Turbulence modelling in CFD, DCW industries, 1994

Appendices

A. Measuring with an Acoustic Doppler Velocimeter (ADV)

B. Modelling the bowthruster

C. Description of a capillary surface wave in the physical model

D. Table with the measurement results.

A. Measuring with an Acoustic Doppler Velocimeter (ADV)

The measurements for this master thesis were done with an ADV (Acoustic Doppler Velocimeter). It was the first time this instrument was used to measure a velocity field. Therefore, experience gained during the measurements is reported. A description of the instrument and the way it works will be given as well as some ways to produce the needed seeding.

Before the measurements in the model of the bowthruster against a quay-wall were done, the instrument was tested in a flume. Simultaneous measurements with the ADV and a LDA (Laser Doppler Anemometry) revealed that measurements were of a similar quality. Unfortunately, during the project the measured data were lost. One graph is all that remained from these measurements. The main goal of these measurements was to gain some experience with the instrument and to make an assessment on the accuracy of the gathered data. The accuracy was far better as was hoped for at the beginning of the project, so the decision was made not to repeat the measurements. With the measurements in the flume, a different type of seeding was used then the measurements in the physical model. Because this type of seeding looks promising for future measurements, this method is described in the section about the hydrogen bubbles.

A.1 Description of the ADV

An ADV measures the flow velocity of the fluid on the particles it transports. The instrument emits a sonic pulse. This pulse reflects on particles in the measurement volume. The echo will be received in the sensors placed to the side of the emitting point (see Figure 42). The reflected signal has a Doppler-shift that determents the velocity. By receiving the signal on different locations, the velocity in different directions can be measured. This gives the ADV the possibility to measure a three-dimensional velocity vector.

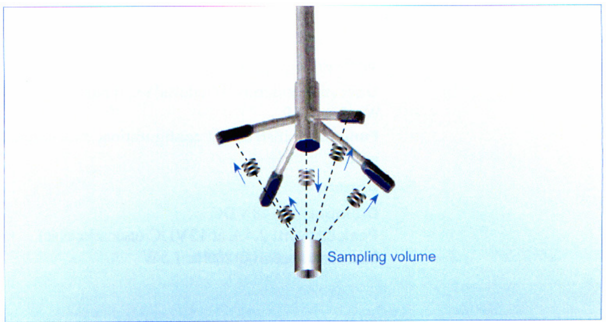

Figure 42: Principle of measuring (from manual of the ADV)

When we look at one measured velocity component, it is measured at an angle of 15° to the z-axis of the instrument. This is exactly half the angle between the emitting point and the receiving point from the centre of the measurement volume. With a minimum of three different velocity components, the size and direction of the flow is fully determined. It is obvious that because of the small angle of the measured velocity components with the z-axis of the instrument, the measured velocity in this direction of the instrument is more accurate than the velocities perpendicular to it. This also shows the restrictions of the velocity range for the different nominal velocities.

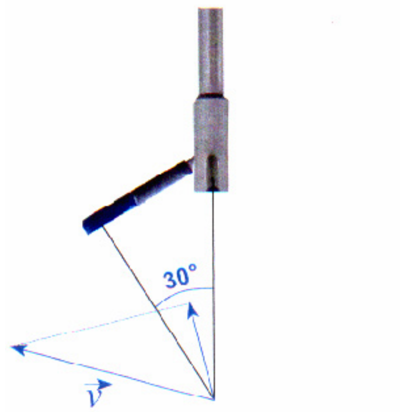

Figure 43: Measured velocity vector (from manual of the ADV)

Of great influence on the accuracy of the measurements are the configuration options. The first option discussed, is the nominal velocity. This option sets the range of the instrument. Hereby it also influences the accuracy of the instrument. The instrumental error is 0.5% (±1 mm/s) of the maximum velocity range. Because of the angle used for measuring the velocity components, the maximal velocity range differs in value for the horizontal and vertical velocities. The range and error in the horizontal direction are larger than the vertical direction of the instrument. For most measurements, the aim is to measure the velocities with the highest accuracy. Therefore, the velocity range should be as low as possible without restricting the measured values. Below a table is given with the velocity range for every configuration value of the nominal velocity.

Nominal velocity [m/s]	*Maximum velocity [m/s]*	
	x- and y-direction	*z-direction*
0.03	0.26	0.08
0.1	0.44	0.13
0.3	0.94	0.27
1.0	1.88	0.54
2.5	3.28	0.94
4.0	5.25	1.50

The next two options influence the measurement volume of the instrument. According to the manufacturer, the measurement volume is of a cylindrical shape with a fixed diameter of 6 mm. The height of the cylinder is adjusted with the transmit length and sampling volume height configurations. The transmit length is a value of the length of the sound pulse. The sampling length is a value for the size of the echo part used to measure the velocities. When these options are altered, the signal strength will also be influenced. Be aware that for a smaller measurement volume or a shorter sample length the instrument needs more seeding. Below is a table with all possible settings for the instrument.

Transmit length (mm)	*Sampling volume height (mm)*				
0.3	1.0	2.5	4.0	5.5	7.0
0.6	1.3	2.8	4.3	5.8	7.3
1.2	1.9	3.4	4.9	6.4	7.9
1.8	2.5	4.0	5.5	7.0	8.5
2.4	3.1	4.6	6.1	7.6	9.1

In the system configurations menu, it is possible to save velocity vectors in a xyz-coordinate system or in a beam coordinate system. The beam coordinate system gives the measured values of each sensor separately. In the xyz-coordinate system, these are recalculated to an orthogonal system with a fixed orientation to the instrument. See the figure below.

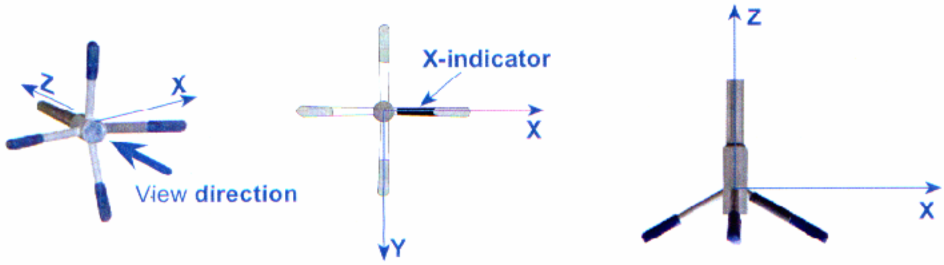

Figure 44: Orientation of the xyz-coordinate system in reference to the instrument (from the manual of the ADV)

A.2 Creation of seeding

As earlier stated, the instrument needs seeding to be able to measure a velocity. The particles of the seeding material reflect the sound pulse needed for measuring. That is why the size of the particles is important. They need to be of a certain magnitude to be able to reflect the sound pulse. Unimportant is the type of material, as long it is capable of producing an echo of the sound pulse in water. It is possible to use sediment, microorganisms and bubbles as seeding material. Below there is a description of hydrogen bubbles and sediment for using as seeding material.

The theoretical needed particle size:

From the sound speed and frequency, the length of the sound wave can be calculated. This length is important to assess the minimal required size of a particle, which is still able to reflect the sound signal.

Frequency of the sound pulse: 10,000,000 Hz (= 10 MHz)
Speed of sound in water (20°C): 1484 m/s
Length of sound wave: $1484/10^7 = 1.484*10^{-4}$ m = 0.1 mm

This means that the seeding material needs to have a minimum particle size of approximately 50 μm (halve the length of the sound wave) to be able to reflect the transmitted signal.

A.2.1 Hydrogen bubbles

For the simultaneous measurements with the ADV and the LDA, a seeding of hydrogen bubbles was used. The water system in the laboratory is a closed system. Most types of seeding are very hard to remove. Optic measurement instruments used in the laboratory need clear water to be able to measure. The seeding necessary to measure with an ADV makes the water less transparent. During the simultaneous measurements, there was a very small seeding range were both instruments were just able to measure. The signal strength of the ADV was very low while the laser of the LDA had just enough strength to produce a measurement signal because the water was not clear enough. However, the seeding with gas bubbles will finally dissolve in the water, or flee the water at the surface. Re-use of the water in other flumes with optic measurement instrument should not be a problem.

A disadvantage with the use of gas bubbles is the flow disturbing bubble generator. To make the bubbles, a frame is needed upstream of the ADV instrument. This can result in measuring additional turbulence from the frame. A wrong placement can also cause the measuring of an offset velocity spectrum. If the bubble concentration varies in the velocity spectrum, the instrument will measure the velocity of the high concentration. The signal of this part of the flow is stronger. It will dominate the measurement giving an excentric data series of the situation especially; the use of a filter for the signal strength can exert this phenomenon. However, this can also occur with other types of seeding and belongs to the properties of the ADV instrument.

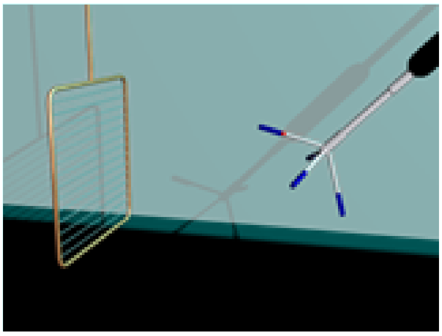

Figure 45: Measuring with a bubble frame. This set-up was used during the simultaneous measurements with the LDA

As earlier stated, the hydrogen bubbles will be made with a bubble frame. This frame produces the bubbles by electrolyse. The hydrogen bubbles on the cathode (-) and oxygen bubbles on the anode (+). See reaction equation below:

$$2\,H_2O + \text{DC (direct current)} \rightarrow 2\,H_2 + O_2 \qquad \textbf{(A.1)}$$

The equation suggests that the volume of hydrogen produced is larger as the volume of oxygen. The size of the bubbles is comparable to the size of the wires used to produce them. In the frame used for the ADV test, 0.2 mm copper wires within a frame of a thicker copper wire (Figure 45) made the bubbles. The surrounding copper wire was coated with wax to prevent it from producing large bubbles. In other projects, it was possible to produce hydrogen bubbles with platinum wires of the size 25-50 μm. If in the future a new frame is constructed, it deserves some research to minimize the thickness of the wire. According to the theoretical size of the particles, hydrogen bubbles of the size 50 μm are as good as the bigger bubbles. Smaller bubbles, also means that with the same amount of energy more bubbles are produced. Another advantage of smaller bubbles is that the raising speed of the bubbles will be smaller and there for it will have less influence on the measurements. This could be of great importance with measurements in slow or low turbulent currents, where the frame cannot be placed very close to the ADV instrument.

During the simultaneous measurements, the bubbles from the small wires became bigger when a white substance accumulates on it. Possibly this was a reaction with one of the unknown salts in the water. When an attempt is made to make a better wire frame it is advisable to research the possibilities to prevent the substance accumulating on the wires, or find a way to remove it.

A solution needs to be found for measurements near the bottom. The highest signal strength was measured straight behind the centre of the bubble frame. When a measurement near the bottom is made, only the bubbles from the lowest few wires could reach the measurement volume. The signal strength was in these situations very low. For these kinds of measurements, it could be better to produce the seeding on a wire frame that is placed flat on the bottom. This way the concentration of the bubbles on the bottom be comes higher.

A.2.2 Sediment

Before the measurements in the closed model started, some different possible seeding materials were tried out. Below is a description of the different materials and the findings during some tests.

Material	*Particle size*	*Remarks*
Vectrino seeding material	~10 μm	Material works well. However, a lot of material is used for a small amount of water. Seeding the whole basin (~19 m^3) required more material as was available.
Kaolin	~10 μm	Material is too heavy. In the tests, before the measurements, the material sank very quickly to the bottom.
Illite (a type of fine clay)	~1-100 μm	There is a need for a lot of material. After some time, the strength of the signal decreases, due to sinking of the needed size seeding material. The large amount of fine material makes the water look very dirty.
Latex	1 μm	Material is probably too fine. The ADV was unable to measure during the tests.

A.3 Accuracy of measurements

According to the manufacturer, the measurements have an accuracy of 0.5% of the maximum velocity (±1 mm/s). The accuracy is therefore largely dependent on the configuration of the instrument, as is stated before. Besides the instrumental fault, there can also be a measurement fault. The instrument does not measure on the water itself. The velocity of the suspended particles is measured. This is assumed to be the same as the velocity of the water. When the particles have a relative velocity to the flow, due to sinking or buoyancy of the particles, this is not true.

When the measurements of the ADV are compared with simultaneously measurements of a LDA, the results are almost the same, as shown in figure below. Some remark on the measurements of this figure must be made. The location of measuring for the LDA and the ADV was not exactly the same. The measurement point of the LDA was placed 1 cm behind the ADV. In addition, the offset of the LDA is not corrected, as well as the orientation difference. The results are, despite these inaccuracies, very well comparable. No notice should be taken the two measurement points of the LDA near the bottom. These measurements were done on a bad signal, due to dirt on the glass walls.

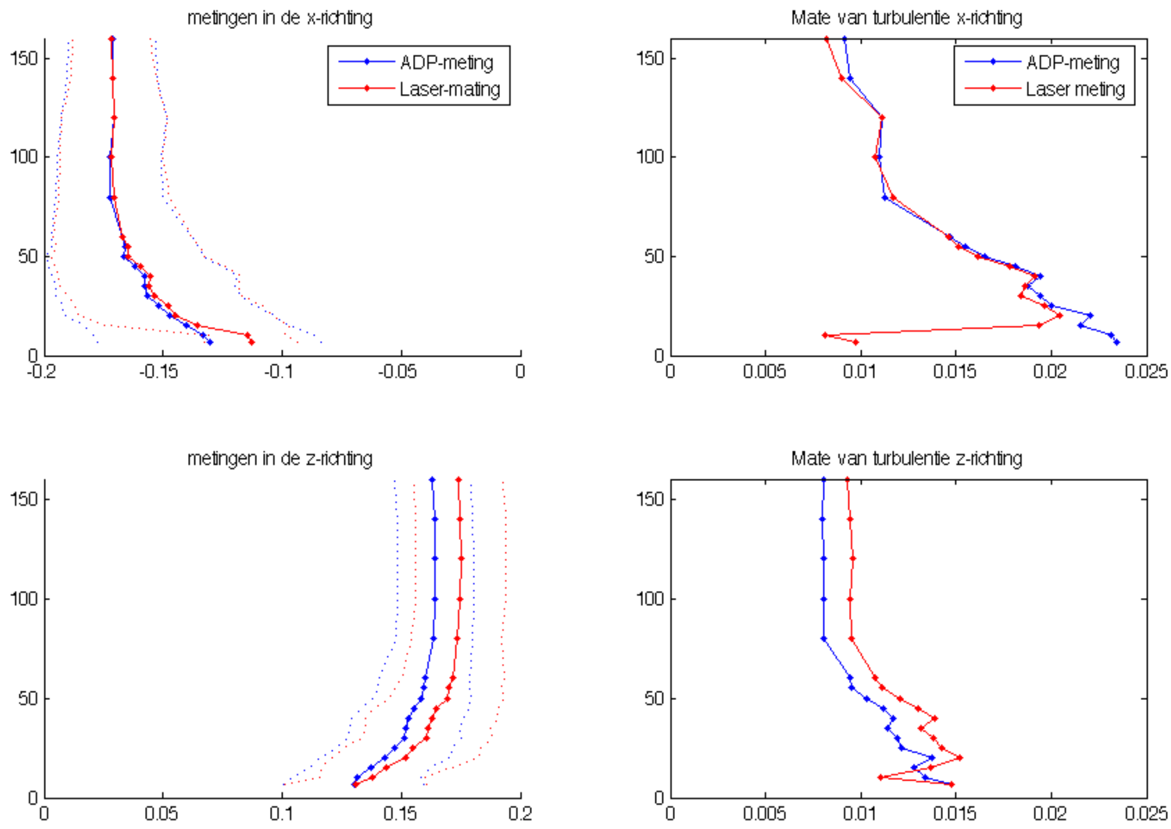

Figure 46: Simultaneous measurements of a LDA and ADV. The orientation of the instruments is on a 45-degree angle with the flow direction.

A.4 Processing the data

From the measured velocities, different flow characteristics can be determined. These characteristics all present a property of the flow. To show the possibilities of the ADV, the characteristics of the flow, calculated during the project, are treated below.

Average velocity:

$$U_{m,i} = \overline{U_i} \quad \text{[m/s]} \tag{0.1}$$

where:

U_i = The measured velocities in the i-direction [m/s]

$U_{m,i}$ = Mean velocity in the i-direction [m/s]

Standard deviation of the velocity:

$$\sigma_i = \sqrt{\overline{\left(U_i - \overline{U_i}\right)^2}} \quad \text{[m/s]} \tag{0.2}$$

where:

σ_i = Standard deviation of the measured velocities in the i-direction [m/s]

Reynolds stresses:

It is possible to calculate the Reynolds stresses from the turbulence velocities. Reynolds averaging results in six stresses, three shear stresses and three normal stresses. The definition of these stresses can be used to estimate the turbulence by means of a velocity measurement. They give a value of the momentum exchange in the different directions.

$$\tau_{ij} = -\rho \cdot \overline{U'_i \cdot U'_j} \quad \text{[N/m}^2\text{]} \tag{0.3}$$

where:

τ_{ij} = shear stress on the ij-plane [m/s]

ρ = density of the fluid [kg/m^3]

Turbulent energy:
Another turbulence characteristic is the turbulent energy. This characteristic is used for comparisons with computational turbulence models. The turbulent energy can be obtained by calculating the contribution for every stress direction. Alternatively, by calculating a total value of the turbulent energy regardless the direction. The last one is used for comparing with viscous turbulence models.

$$k_{ij} = \tfrac{1}{2}\rho \cdot \overline{U_i{'} \cdot U_j{'}} \text{ [J/m}^3\text{]} \quad \textbf{(0.4)}$$

$$k_t = \tfrac{1}{2}\rho \cdot \overline{U_t{'}^2} \text{ [J/m}^3\text{] with } U'_t = \sqrt{U'^2_i + U'^2_j + U'^2_k} \text{ [m/s]} \quad \textbf{(0.5)}$$

where:
k_{ij} = Turbulent energy through the ij-plane [J/m^3]
k_t = Total turbulent energy [J/m^3]

Before calculating any of these characteristic values, it is possible to filter the data. The output file contains besides the velocity data and for every measurement some additional information. This information gives values of the signal strength, the signal-to-noise ratio and the correlation coefficient. They tell something about the rightness of the measurements. With applying filters on these values, bad data can be filtered out.

A.5 Checklist

During the measurements, some experience on measuring with an ADV was gained. If the measurements are done with great care, the results can be as good as that of a LDA. However, it is also possible, as with every measurement instrument, to produce wrong results. To summarise the experience and to give others a guideline to make good measurements, the checklist below was made.

Before the measurements	
Is the instrument mounted properly? The instrument should be mounted properly. The flow should not be able to move the instrument to prevent that the vibrations will be measured as additional turbulence.	Yes / No
Is the seeding apparatus rightly aligned and turned on? If a bubble frame is used for the seeding, the flow should transport the bubbles to the measurement location. When this is not the case, there will be no, or a very bad signal for measuring the velocities. This shows as a noisy signal. This is also produced when the instrument is out of the water.	Yes / No
At the start of each measurement	
Orientation of the instrument Document how the instrument is positioned. This could be important for the analysis.	Values
Instrument configurations Nominal velocity (see par. A.1 for advise) Measurement volume (see par. A.1 for advise) Signal strength (see par. A.1 for advise)	 Value Value Value
During the measurements	
To keep an eye on: Signal strength (minimum of 70 counts is advise by the manufacturer) Measurement restrictions (maximum velocity, see par. A.1)	
Data analysis	
Converting the data In the past, for unknown reasons, the program made mistakes converting the data. This could be seen in the header file. Here the nominal velocity sometimes deviated from the real used nominal velocity. In these cases, the program was restarted and the file reconverted. Most times this solved the problem.	
Data analysis Filtering the data and correcting for the orientation of the instrument	

B. Modeling the bowthruster

The information in the report over the way the bowthruster was modeled in the numerical model is a bit scattered. This appendix is written to summarize and extend the information about the critical aspect of the numerical model. It was a request from the thesis committee at the presentation of the research in Delft.

B.1 Bowthruster in the physical model

In this paragraph, a description is given of the situation in the physical model. The bowthruster is a pipe through the hull of the ship. In the middle of the pipe a model screw is placed. This screw is not an exact scaled version of a real screw (specification, see figure). Therefore the flow properties can differ from prototype situations. The screw is powered by an electric motor. The motor drives the screw with a rubber string to a wheel on the screw axis.

Properties of the model screw:

Brand: Raboesch
Type: 167-31 R M5
Propeller diameter: 0.10 m
Number of blades: 4 [-]
Material: brass
Motor rpm, during the measurements: 850

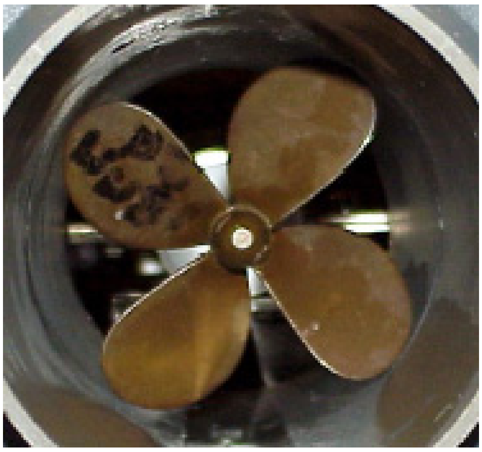

Figure 47: Screw in the bowthruster

B.2 Bowthruster in the numerical model

In the numerical model, the bowthruster is build as a fan. This fan is placed as a propeller in the ship. Some solid fills act as guidance and form together the pipe of the bowthruster (see figure below).

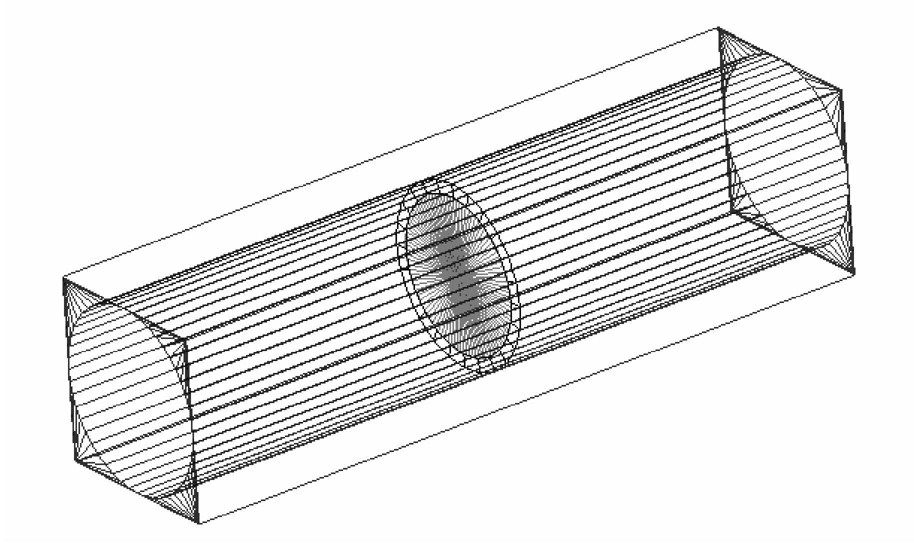

Figure 48: Bowthruster of the adapted numerical model

The fan is the source of the flow in the model. It forces a velocity on the area of a ring in the bow-thruster. A centre plate inside this ring blocks the centre. This is normally the location of the screw axis. The size of this plate is large, when it is compared to the real size of the screw axis in the physical model. The uniform velocity that is forced on the ring area of the screw could have played a role in this. Real screws do not force a uniform flow on the screw. The velocities at the outer side of the screw are higher as near the axis. This velocity gradient perpendicular to the screw axis is not forced in the model. The addition of a lager axis plate partially solves this difference.

Besides this, the screw does not seem to have any turbulence production in it. The turbulence in the calculations is produced by the velocity differences in the bowthruster and at the walls. This means, that the addition of a turbulence source in the screw, could have a large impact on the calculations and will be necessary for calculating the correct turbulent properties of the flow.

B.2.1 Swirl number

The swirl number is the ratio between the rotational speed and the averaged axial velocity of the screw. The averaged axial velocity is the velocity that is forced by the screw along the axis. De Jong suggested the first value of the swirl number. He found a value of 0.8 based on the measurements of Schokking. The measurements in the bowthruster model for this thesis confirmed this value of the swirl number (see Figure 34).

B.2.2 Size axis plate

The size of the axis plate corrects for the assumption in the numerical model of an averaged axial screw velocity. A real-life screw gives the flow at the end of the propeller blades a higher velocity as close to the screw axis. This is not in the numerical model. Applying a lager blockade in the centre, forces a larger low-velocity core. Diffusion of the flow velocities, result in a comparable outflow distribution to the physical model.

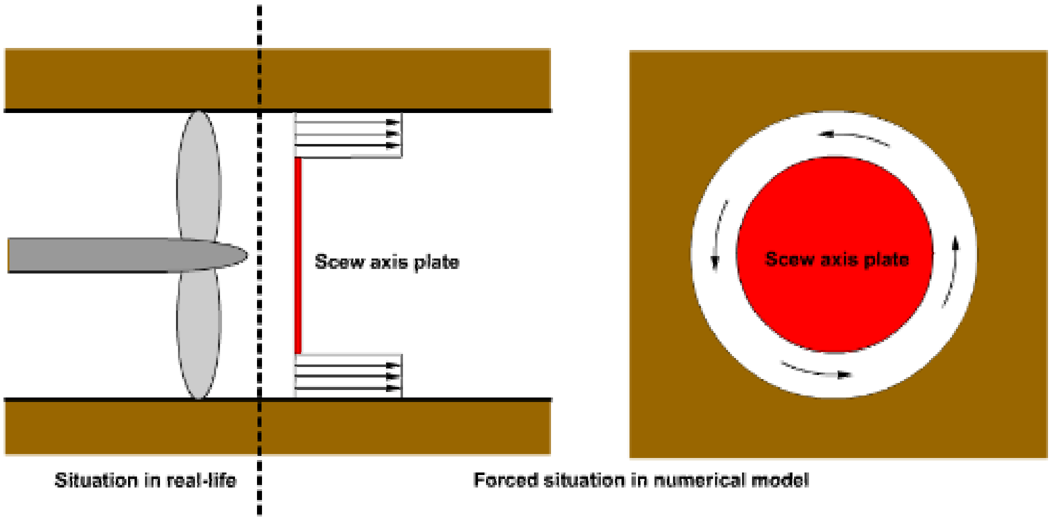

Figure 49: Visualisation of the bowthruster in the numerical model

De Jong suggested a size of the axis plate with a diameter of 30% of the bowthruster diameter. He based this on the measurements of Schokking. In the measurements of the bowthruster model, it shows to be too small. An axis plate with a diameter of 85% of the bowthruster diameter was needed to match the outflow measurement results of the physical model. This could have an origin in the grid size of the numerical calculations or the turbulence production in the thruster. The influences of these parameters are not assessed in the sensitivity analyses of the numerical model. When this is done, it is advisable to model a smaller part of the current numerical model. Otherwise, the calculation time will increase extensively.

B.2.3Turbulent intensity

In the Q1-file, a number for the turbulent intensity is adaptable. The standard value of this parameter is 5.0%. However, this value can be defined; trials show, that the software does not use this value in the calculations. This results in no production of turbulence in the screw of the bowthruster.

B.2.4 Implementing a turbulence source

It should be possible to ad a turbulence source in the screw of the numerical model. However this needs some extra efforts for doing. The turbulence source must be defined in the Q1-file and it is not easily done.

Another way of modeling the bowthruster is also possible. The propeller can be modeled as a solid with an inflow and an outflow boundary. This way it is possible to create a turbulent inflow boundary for simulating the turbulent flow properties of the screw. The swirl must also be put into the outflow boundary (inflow of the bowthruster), to retain rotational inflow.

Below, the table gives a description of the screw in the numerical model.

Screw geometry of De Jong (2003)		**Adapted screw geometry**	
NAME,	SCHROEF	NAME,	SCHROEF
POSITION,	4.3, 2.9, 0.16	POSITION,	4.3, 2.9, 0.16
SIZE,	0, 0.1, 0.1	SIZE,	0, 0.1, 0.1
GEOMETRY,	cylpipe	GEOMETRY,	cylpipe
ROTATION24,	9	ROTATION24,	9
GRID,	NO	GRID,	NO
TYPE,	FAN	TYPE,	FAN
VOLUFLOW,	3.500000E-03	VOLUFLOW,	3.500000E-03
PRESSURE,	0.000000E+00	PRESSURE,	0.000000E+00
TURB-INTENS,	5.000000E+00	TURB-INTENS,	5.000000E+00
DIAMRATI,	3.000000E-01	DIAMRATI,	8.500000E-01
SWIRLNUM,	8.000000E-01	SWIRLNUM,	8.000000E-01
SWIRLDIR,	1.000000E+00	SWIRLDIR,	1.000000E+00
FANAXISD,	1.000000E+00	FANAXISD,	1.000000E+00

C. Description of a capillary surface wave in the physical model

During the measurements, a small wave appeared at the water surface. This very small standing wave separated the clean water-surface from the water surface with floating particles. The part of the surface with the floating particles seemed to have no residual velocity, besides the turbulence vortices that moved the particles around. Adding a tracer revealed that the water just below the surface passed the wave without any hinder. With earlier measurements, this wave was not noticed. An explanation for the phenomenon is not present.

It seems to be clear that the phenomenon has something to do with surface tension. The addition of a soap to remove the dirty film on the surface resulted in the disappearing of the wave. After a few seconds, the wave reappeared, starting at the wall and growing to its original location, this time in a clear water surface on both sides of the wave.

The velocity of the flow, at the location of the wave is estimated to be approximately 0.04 m/s. This is a calculated guess, from the location, the velocity in the calculations, and the used rpm of the motor. Measurements were not done at this location.

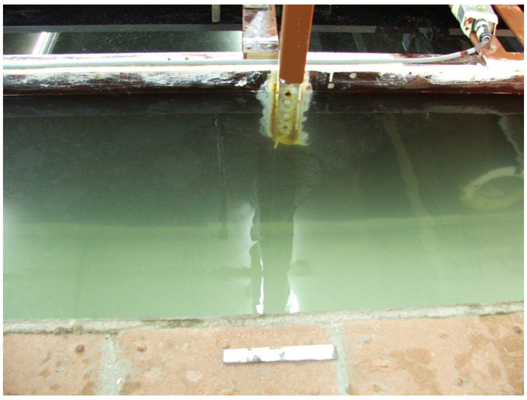

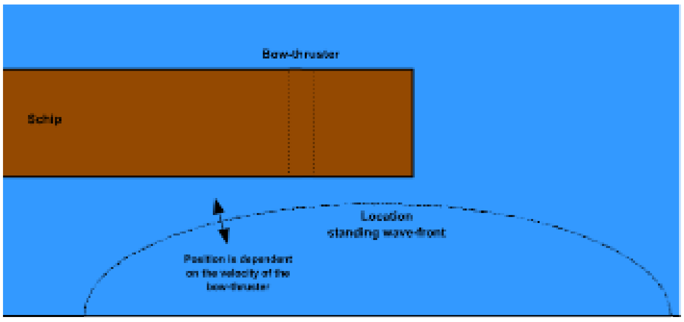

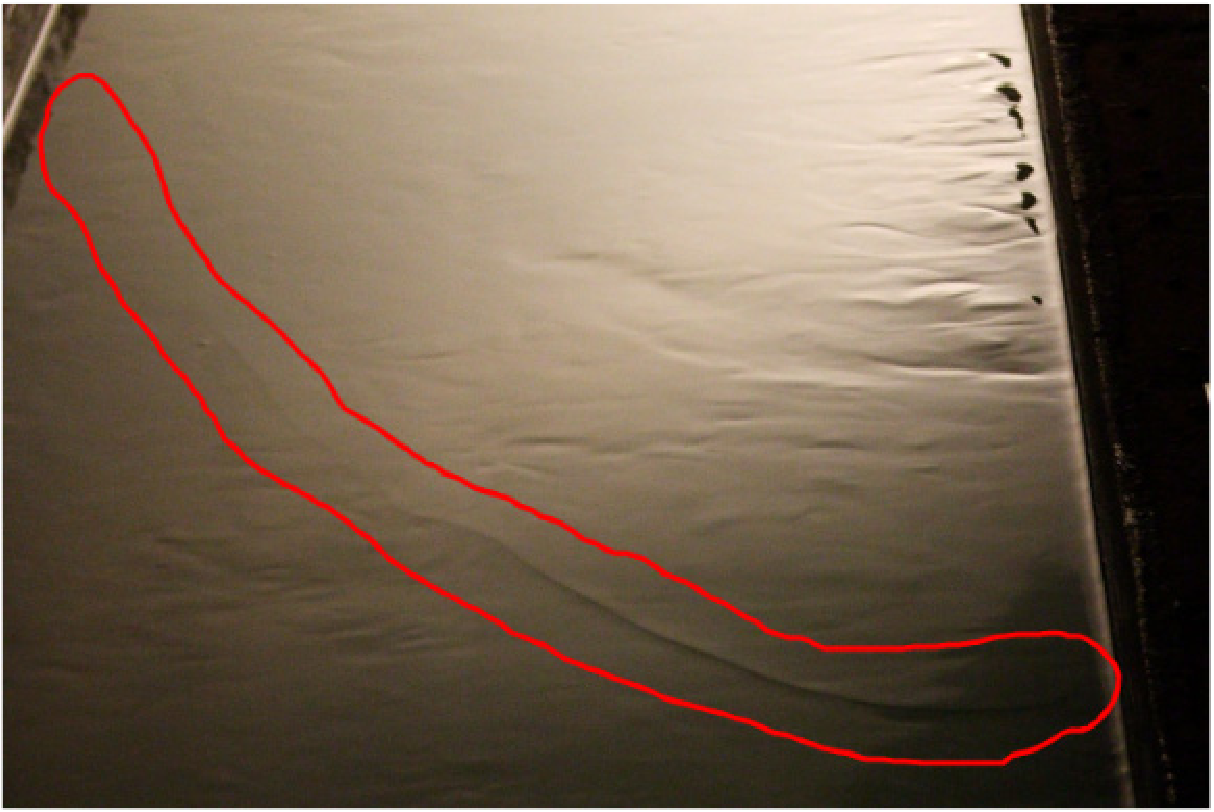

D. Table with the measurement results

The measurements were done is three series. An explanation for the measurement points is given in chapter 5. The results are below, in no particular order.

x [m]	y [m]	z [m]	U [m/s]	u [m/s]	v [m/s]	w [m/s]	ke [J/m3]	quu [N/m2]	quv [N/m2]	quw [N/m2]	qvv [N/m2]	qvw [N/m2]	qww [N/m2]
4.500	1.000	0.015	0.026	0.024	0.006	-0.007	0.093	-0.030	-0.011	-0.016	-0.099	-0.008	-0.057
4.500	1.000	0.030	0.026	0.021	0.008	-0.014	0.156	-0.063	-0.001	-0.026	-0.142	-0.009	-0.107
4.500	1.000	0.045	0.035	0.014	0.011	-0.030	0.392	-0.279	-0.062	-0.119	-0.339	0.017	-0.166
4.500	1.300	0.015	0.028	0.023	0.012	-0.010	0.177	-0.063	-0.009	-0.037	-0.157	0.007	-0.135
4.500	1.300	0.030	0.032	0.022	0.012	-0.019	0.185	-0.062	-0.013	-0.034	-0.128	0.006	-0.179
4.500	1.300	0.045	0.030	-0.003	0.002	-0.030	0.322	-0.245	0.002	-0.178	-0.138	0.044	-0.263
4.500	1.600	0.015	0.027	0.023	0.004	-0.012	0.208	-0.078	-0.010	-0.053	-0.180	0.011	-0.159
4.500	1.600	0.030	0.034	0.026	0.008	-0.020	0.408	-0.179	-0.115	-0.131	-0.365	-0.111	-0.272
4.500	1.600	0.045	0.037	0.017	0.001	-0.032	0.181	-0.061	-0.012	-0.037	-0.133	0.015	-0.169
4.500	1.900	0.015	0.024	0.020	-0.001	-0.013	0.248	-0.082	-0.007	-0.048	-0.205	0.009	-0.209
4.500	1.900	0.030	0.028	0.021	-0.003	-0.018	0.225	-0.085	-0.009	-0.051	-0.153	-0.007	-0.212
4.500	1.900	0.045	0.024	0.020	-0.005	-0.012	0.244	-0.103	-0.004	-0.042	-0.199	-0.000	-0.187
4.500	2.100	0.015	0.026	0.019	-0.011	-0.014	0.292	-0.106	-0.035	-0.064	-0.230	-0.017	-0.249
4.500	2.100	0.030	0.032	0.018	-0.010	-0.024	0.272	-0.093	-0.019	-0.048	-0.207	0.007	-0.245
4.500	2.100	0.045	0.024	0.017	-0.008	-0.016	0.292	-0.107	-0.018	-0.065	-0.219	-0.031	-0.259
4.500	2.300	0.015	0.025	0.010	-0.018	-0.014	0.256	-0.100	-0.002	-0.044	-0.214	0.016	-0.198
4.500	2.300	0.030	0.027	0.010	-0.015	-0.020	0.304	-0.118	0.019	-0.031	-0.231	-0.023	-0.259
4.500	2.300	0.045	0.032	0.007	-0.014	-0.028	0.302	-0.089	-0.013	-0.031	-0.276	0.013	-0.238
4.500	2.400	0.015	0.021	0.009	-0.018	-0.008	0.262	-0.086	-0.008	-0.049	-0.239	-0.018	-0.198
4.500	2.400	0.030	0.019	0.008	-0.012	-0.012	0.263	-0.106	-0.011	-0.003	-0.196	-0.007	-0.224
4.500	2.400	0.045	0.019	0.005	-0.012	-0.014	0.248	-0.072	-0.002	-0.002	-0.222	-0.008	-0.203
4.500	2.500	0.015	0.024	0.010	-0.021	-0.005	0.184	-0.081	-0.004	-0.013	-0.167	-0.001	-0.119
4.500	2.500	0.030	0.020	0.006	-0.019	-0.005	0.195	-0.109	0.006	-0.004	-0.159	0.012	-0.122
4.500	2.500	0.045	0.014	0.001	-0.013	-0.006	0.196	-0.076	0.002	0.029	-0.096	0.008	-0.220
4.500	2.800	0.015	0.038	-0.016	-0.034	0.001	0.161	-0.128	0.036	-0.037	-0.125	0.018	-0.069
4.500	2.800	0.030	0.038	-0.017	-0.033	0.005	0.131	-0.096	0.017	-0.031	-0.088	0.004	-0.078
4.500	2.800	0.045	0.039	-0.024	-0.029	0.009	0.147	-0.106	0.009	-0.022	-0.105	0.017	-0.084
4.500	3.000	0.015	0.073	-0.064	-0.034	0.002	0.429	-0.297	-0.004	-0.070	-0.358	-0.003	-0.204
4.500	3.000	0.030	0.071	-0.063	-0.033	0.000	0.428	-0.317	-0.022	-0.022	-0.347	0.003	-0.193
4.500	3.000	0.045	0.057	-0.041	-0.039	0.011	1.725	-2.156	0.000	-1.089	-0.525	0.044	-0.770
4.500	3.100	0.015	0.053	-0.047	-0.023	0.002	0.255	-0.138	-0.050	-0.039	-0.270	-0.026	-0.104
4.500	3.100	0.030	0.050	-0.046	-0.019	0.003	0.248	-0.147	-0.039	-0.015	-0.241	-0.009	-0.109
4.500	3.100	0.045	0.029	-0.011	-0.015	0.022	0.829	-0.939	0.012	-0.559	-0.254	0.050	-0.466
4.500	3.200	0.015	0.034	-0.032	-0.012	0.001	0.123	-0.090	-0.010	-0.019	-0.108	-0.000	-0.047
4.500	3.200	0.030	0.034	-0.033	-0.009	0.002	0.182	-0.185	-0.017	-0.039	-0.119	-0.006	-0.059
4.500	3.200	0.045	0.018	-0.010	-0.005	0.014	0.590	-0.716	-0.009	-0.402	-0.130	-0.001	-0.332
4.500	3.300	0.015	0.035	-0.033	-0.012	0.000	0.158	-0.150	-0.007	-0.016	-0.117	0.002	-0.049
4.500	3.300	0.030	0.033	-0.031	-0.012	0.001	0.128	-0.105	0.004	-0.006	-0.106	-0.001	-0.044
4.500	3.300	0.045	0.031	-0.031	-0.003	0.001	0.232	-0.278	-0.020	-0.063	-0.135	-0.006	-0.052
4.500	3.400	0.015	0.036	-0.025	-0.025	-0.000	0.102	-0.087	0.001	-0.017	-0.080	-0.005	-0.037
4.500	3.400	0.030	0.036	-0.026	-0.025	-0.001	0.130	-0.104	0.002	-0.005	-0.103	0.007	-0.052
4.500	3.400	0.045	0.033	-0.023	-0.024	-0.000	0.328	-0.254	-0.024	0.009	-0.240	0.041	-0.161
4.500	3.500	0.015	0.037	-0.026	-0.027	0.002	0.136	-0.095	0.032	-0.014	-0.131	-0.007	-0.046
4.500	3.500	0.030	0.040	-0.030	-0.026	0.004	0.088	-0.053	0.008	-0.008	-0.090	-0.000	-0.032
4.500	3.500	0.045	0.037	-0.029	-0.022	0.003	0.181	-0.106	0.032	-0.005	-0.178	-0.005	-0.078
4.500	0.400	0.015	0.025	0.024	0.003	-0.007	0.078	-0.023	0.006	-0.007	-0.102	-0.021	-0.032
4.500	0.400	0.030	0.024	0.021	0.008	-0.010	0.102	-0.039	-0.020	-0.014	-0.099	-0.020	-0.065
4.500	0.400	0.045	0.030	0.008	0.007	-0.028	0.294	-0.339	-0.001	-0.189	-0.099	-0.009	-0.150
4.500	0.700	0.015	0.024	0.022	0.008	-0.006	0.095	-0.039	-0.021	-0.017	-0.098	-0.020	-0.053
4.500	0.700	0.030	0.026	0.022	0.008	-0.011	0.096	-0.043	-0.006	-0.025	-0.102	-0.014	-0.048
4.500	0.700	0.045	0.024	0.016	0.007	-0.017	0.118	-0.040	-0.019	-0.023	-0.134	-0.027	-0.063
4.550	2.950	0.110	0.036	0.020	-0.007	0.029	1.751	-0.980	0.120	-0.023	-1.538	0.357	-0.985
4.550	2.950	0.015	0.065	0.058	0.029	0.006	0.416	-0.465	0.081	-0.030	-0.212	0.072	-0.155
4.550	2.950	0.160	0.616	0.496	0.345	-0.123	30.079	-28.468	-11.720	-10.076	-16.830	-3.019	-14.860
4.550	2.950	0.185	0.062	0.027	0.033	-0.044	20.071	-13.381	1.006	-5.217	-12.876	2.137	-13.885
4.550	2.950	0.210	0.013	-0.007	-0.007	0.009	20.290	-11.997	1.618	1.429	-14.627	2.612	-13.957
4.550	2.950	0.235	0.333	0.247	-0.219	0.047	79.835	-90.848	20.482	-14.740	-39.003	17.494	-29.818
4.550	2.950	0.260	0.447	0.363	-0.237	0.107	51.128	-36.316	7.291	-13.091	-26.763	26.696	-39.177
4.550	2.950	0.030	0.071	0.064	0.028	0.011	0.694	-0.902	0.055	0.037	-0.272	0.087	-0.213
4.550	2.950	0.325	0.048	-0.006	0.003	-0.047	1.831	-0.996	-0.219	0.322	-1.150	1.055	-1.515
4.550	2.950	0.375	0.038	-0.008	-0.003	-0.037	1.468	-0.941	-0.336	0.420	-0.907	0.745	-1.088
4.550	2.950	0.450	0.032	-0.003	-0.005	-0.032	0.712	-0.474	-0.080	0.124	-0.509	0.244	-0.442
4.550	2.950	0.550	0.025	-0.010	-0.008	-0.022	1.145	-1.137	0.159	-0.106	-0.586	0.279	-0.568
4.550	2.950	0.060	0.029	0.028	0.006	0.007	1.363	-1.227	0.128	-0.163	-0.753	0.180	-0.746
4.600	2.950	0.110	0.087	0.083	0.019	0.018	19.036	-12.526	-0.206	0.440	-8.367	6.840	-17.179
4.600	2.950	0.015	0.057	0.050	0.027	0.007	0.401	-0.433	0.076	-0.020	-0.233	0.091	-0.136
4.600	2.950	0.160	0.301	0.211	0.214	0.005	46.905	-45.457	-1.352	-6.180	-21.292	10.506	-27.062
4.600	2.950	0.185	0.151	-0.087	0.120	-0.027	23.293	-15.190	-0.866	-2.327	-14.857	6.445	-16.539
4.600	2.950	0.210	0.115	-0.088	-0.059	-0.045	21.981	-14.591	0.973	-0.045	-13.906	5.322	-15.464
4.600	2.950	0.235	0.225	0.124	-0.185	-0.031	46.726	-45.660	4.960	0.759	-24.369	9.785	-23.422
4.600	2.950	0.260	0.456	0.410	-0.198	0.030	40.714	-27.555	8.657	-11.914	-16.908	16.886	-36.964
4.600	2.950	0.030	0.055	0.045	0.029	0.010	0.491	-0.532	0.103	-0.045	-0.236	0.076	-0.214
4.600	2.950	0.325	0.046	-0.010	-0.021	-0.040	1.305	-0.946	-0.059	0.057	-0.841	0.415	-0.822
4.600	2.950	0.375	0.032	-0.011	-0.010	-0.029	0.517	-0.339	-0.089	0.036	-0.500	0.040	-0.195
4.600	2.950	0.450	0.021	-0.013	-0.008	-0.015	0.426	-0.212	0.006	-0.001	-0.526	0.003	-0.114
4.600	2.950	0.550	0.019	-0.015	-0.010	-0.002	0.484	-0.372	0.010	-0.029	-0.367	0.055	-0.229
4.600	2.950	0.060	0.054	0.046	0.021	0.017	0.881	-0.655	0.055	-0.123	-0.526	0.125	-0.580
4.700	2.950	0.110	0.225	0.211	0.078	-0.004	32.584	-31.790	-1.601	5.540	-14.616	10.369	-18.761
4.700	2.950	0.015	0.031	0.017	0.024	0.010	0.942	-0.921	0.048	0.102	-0.579	0.123	-0.384
4.700	2.950	0.160	0.211	0.168	0.127	0.008	19.457	-13.646	0.531	-4.106	-11.647	5.922	-13.622
4.700	2.950	0.185	0.091	0.075	0.050	-0.013	17.607	-9.709	0.732	-1.490	-12.059	3.860	-13.446
4.700	2.950	0.210	0.120	0.091	-0.076	-0.019	18.071	-11.738	2.567	1.585	-11.722	4.111	-12.682
4.700	2.950	0.235	0.255	0.207	-0.147	-0.019	19.359	-15.838	2.613	1.075	-10.145	4.819	-12.734
4.700	2.950	0.260	0.301	0.264	-0.146	0.005	20.156	-16.453	1.659	-2.207	-9.509	5.368	-14.349
4.700	2.950	0.030	0.043	0.036	0.021	0.009	1.301	-1.038	-0.065	0.025	-0.853	0.364	-0.711
4.700	2.950	0.325	0.039	0.023	-0.029	-0.014	4.555	-3.117	0.324	-0.642	-3.056	1.315	-2.937
4.700	2.950	0.375	0.021	-0.006	-0.016	-0.011	0.654	-0.307	-0.014	-0.001	-0.682	0.028	-0.318
4.700	2.950	0.450	0.024	-0.009	-0.023	-0.002	0.361	-0.187	-0.005	0.034	-0.342	0.047	-0.192
4.700	2.950	0.550	0.030	-0.020	-0.022	0.004	0.718	-0.519	0.003	-0.048	-0.526	0.136	-0.391
4.700	2.950	0.060	0.056	0.048	0.025	0.016	6.132	-5.577	-0.205	0.313	-3.161	2.273	-3.525
4.800	2.950	0.110	0.239	0.221	0.081	-0.037	12.835	-10.864	-0.167	-0.096	-6.589	3.967	-8.217
4.800	2.950	0.015	0.056	-0.001	0.056	0.001	4.297	-3.629	-0.023	0.822	-2.354	0.972	-2.612
4.800	2.950	0.160	0.119	0.106	0.054	-0.000	13.810	-13.012	0.303	-2.085	-7.380	3.199	-7.229
4.800	2.950	0.185	0.053	0.052	0.014	0.002	10.313	-8.903	1.006	-1.087	-5.905	1.931	-5.818
4.800	2.950	0.210	0.077	0.067	-0.036	0.014	13.024	-10.898	1.810	-0.236	-7.800	2.811	-7.350
4.800	2.950	0.235	0.169	0.146	-0.080	0.026	14.822	-15.381	1.612	0.367	-6.818	3.111	-7.445
4.800	2.950	0.260	0.238	0.211	-0.103	0.042	12.372	-11.245	1.096	-0.325	-6.011	3.461	-7.489
4.800	2.950	0.030	0.056	0.038	0.041	0.001	4.841	-3.916	-0.007	0.874	-2.638	1.114	-3.128
4.800	2.950	0.325	0.107	0.093	-0.049	0.020	6.945	-4.433	0.762	-1.288	-4.603	2.157	-4.854
4.800	2.950	0.375	0.047	0.029	-0.037	0.000	3.266	-2.188	0.246	-0.388	-2.350	1.303	-1.993

x [m]	y [m]	z [m]	U [m/s]	u [m/s]	v [m/s]	w [m/s]	ke [J/m3]	quu [N/m2]	quv [N/m2]	quw [N/m2]	qvv [N/m2]	qvw [N/m2]	qww [N/m2]
4.800	2.950	0.450	0.029	0.003	-0.028	0.008	0.805	-0.369	-0.062	-0.040	-0.771	0.213	-0.471
4.800	2.950	0.550	0.015	-0.009	-0.011	0.004	0.705	-0.492	-0.012	-0.105	-0.452	0.133	-0.466
4.800	2.950	0.060	0.131	0.122	0.044	-0.020	7.739	-5.378	-0.555	1.432	-4.451	2.615	-5.649
4.900	2.950	0.110	0.132	0.115	0.046	-0.046	7.373	-8.093	-0.061	-0.634	-3.103	1.114	-3.549
4.900	2.950	0.015	0.089	0.040	0.069	-0.040	6.384	-6.087	-0.404	1.220	-3.244	1.352	-3.437
4.900	2.950	0.160	0.017	0.005	0.007	-0.014	5.071	-4.666	0.191	-0.344	-2.862	0.904	-2.614
4.900	2.950	0.185	0.011	0.003	-0.004	-0.010	4.912	-4.364	0.402	-0.123	-2.680	0.698	-2.779
4.900	2.950	0.210	0.014	-0.010	-0.003	-0.009	4.771	-4.208	0.424	0.089	-2.729	0.869	-2.606
4.900	2.950	0.235	0.059	0.048	-0.027	0.020	7.055	-7.477	1.112	0.162	-3.391	1.118	-3.242
4.900	2.950	0.260	0.101	0.082	-0.043	0.041	7.913	-9.053	1.170	0.035	-3.541	1.369	-3.232
4.900	2.950	0.030	0.088	0.060	0.046	-0.046	5.200	-4.502	-0.316	0.942	-2.743	1.131	-3.155
4.900	2.950	0.325	0.160	0.123	-0.056	0.086	6.585	-5.619	0.681	-0.323	-3.356	1.751	-4.195
4.900	2.950	0.375	0.106	0.074	-0.038	0.065	4.764	-3.058	0.496	-0.551	-2.726	1.423	-3.744
4.900	2.950	0.450	0.047	0.026	-0.026	0.029	2.268	-1.384	0.078	-0.093	-1.474	0.791	-1.678
4.900	2.950	0.550	0.032	-0.007	-0.017	0.026	1.338	-1.025	-0.010	0.085	-0.757	0.217	-0.894
4.900	2.950	0.060	0.165	0.139	0.057	-0.069	5.520	-4.936	-0.024	0.418	-2.564	1.029	-3.540
4.950	2.950	0.110	0.048	0.043	0.019	0.010	5.133	-4.868	0.164	0.223	-2.633	0.617	-2.765
4.950	2.950	0.015	0.075	0.052	0.048	-0.024	5.486	-5.589	-0.035	0.046	-2.305	0.939	-3.077
4.950	2.950	0.160	0.025	-0.002	0.012	0.021	4.172	-3.448	0.293	0.398	-2.507	0.610	-2.390
4.950	2.950	0.185	0.028	-0.015	-0.001	0.024	3.817	-3.070	0.245	0.197	-2.222	0.536	-2.342
4.950	2.950	0.210	0.030	-0.016	0.003	0.026	4.165	-3.489	0.458	0.747	-2.232	0.621	-2.609
4.950	2.950	0.235	0.028	-0.011	-0.003	0.026	4.173	-3.963	0.354	0.709	-2.040	0.534	-2.343
4.950	2.950	0.260	0.035	0.009	-0.007	0.033	5.451	-5.752	0.594	0.490	-2.666	0.793	-2.484
4.950	2.950	0.030	0.101	0.085	0.048	-0.027	5.039	-4.664	-0.182	0.212	-2.212	0.669	-3.202
4.950	2.950	0.325	0.117	0.067	-0.039	0.088	6.031	-6.570	0.860	-0.408	-2.680	1.086	-2.812
4.950	2.950	0.375	0.141	0.069	-0.046	0.114	4.491	-4.105	0.394	-0.246	-2.101	0.937	-2.776
4.950	2.950	0.450	0.106	0.034	-0.037	0.094	2.913	-2.186	0.227	0.125	-1.484	0.566	-2.157
4.950	2.950	0.550	0.070	-0.003	-0.017	0.068	5.104	-2.925	-0.502	0.854	-3.032	2.772	-4.252
4.950	2.950	0.060	0.104	0.095	0.041	-0.014	5.153	-4.909	0.134	0.279	-2.226	0.736	-3.171
3.800	2.900	0.210	0.018	0.018	0.000	-0.001	0.005	-0.003	-0.000	-0.001	-0.005	-0.000	-0.002
3.800	3.000	0.210	0.020	0.019	0.005	0.000	0.011	-0.009	0.001	0.003	-0.007	-0.001	-0.007
3.800	3.150	0.210	0.016	0.016	0.005	-0.001	0.010	-0.006	-0.001	0.002	-0.009	-0.001	-0.005
3.900	2.900	0.210	0.025	0.025	0.004	0.000	0.009	-0.004	0.001	0.001	-0.006	-0.001	-0.007
3.900	3.000	0.210	0.023	0.023	0.001	0.000	0.003	-0.003	-0.000	0.000	-0.002	0.000	-0.002
3.900	3.150	0.210	0.018	0.018	0.003	0.001	0.032	-0.014	-0.002	0.006	-0.022	-0.005	-0.028
3.950	2.900	0.210	0.029	0.028	0.004	-0.001	0.013	-0.006	0.001	-0.000	-0.010	-0.000	-0.010
3.950	3.000	0.210	0.026	0.026	-0.001	0.001	0.005	-0.003	-0.001	-0.000	-0.003	0.001	-0.003
3.950	3.150	0.210	0.013	0.010	-0.007	-0.002	0.176	-0.100	-0.051	-0.015	-0.120	0.016	-0.132
4.550	2.850	0.210	0.073	-0.004	0.049	-0.053	1.098	-0.873	-0.015	0.127	-0.725	-0.021	-0.599
4.550	2.900	0.210	0.698	0.583	-0.214	-0.320	20.649	-18.430	1.552	4.881	-11.333	4.081	-11.535
4.550	3.000	0.210	0.626	0.517	0.077	0.345	30.120	-24.567	4.380	-11.241	-18.474	10.615	-17.200
4.550	3.050	0.210	0.062	0.005	-0.037	-0.050	4.229	-3.412	0.016	-0.227	-2.288	1.713	-2.759
4.600	2.850	0.210	0.066	0.006	0.004	-0.066	21.856	-14.873	1.040	-0.764	-18.941	5.517	-9.898
4.600	2.900	0.210	0.405	0.347	-0.070	-0.196	36.437	-31.638	0.210	5.357	-25.911	7.350	-15.325
4.600	3.000	0.210	0.361	0.314	-0.031	0.175	71.754	-75.313	13.529	-9.897	-38.425	11.049	-29.770
4.600	3.050	0.210	0.051	0.032	-0.037	0.013	15.478	-10.704	-0.799	0.197	-11.578	2.263	-8.675
4.600	3.150	0.210	0.031	0.001	-0.021	-0.023	0.816	-0.683	-0.142	0.174	-0.445	0.259	-0.504
4.700	2.850	0.210	0.152	0.127	-0.036	-0.076	18.979	-14.053	5.215	-1.150	-15.543	2.531	-8.362
4.700	2.900	0.210	0.260	0.214	-0.047	-0.139	18.982	-15.594	-0.828	1.932	-14.140	2.511	-8.231
4.700	3.000	0.210	0.284	0.246	-0.027	0.138	21.214	-19.560	2.277	-2.216	-12.239	1.963	-10.629
4.700	3.050	0.210	0.170	0.143	0.000	0.091	18.452	-15.006	-3.453	-0.146	-12.514	1.171	-9.383
4.700	3.150	0.210	0.034	0.009	-0.033	0.001	0.488	-0.238	0.031	0.005	-0.430	0.098	-0.309
4.800	2.850	0.210	0.154	0.124	-0.059	-0.070	30.224	-41.926	1.281	-4.902	-11.198	4.134	-7.325
4.800	2.900	0.210	0.155	0.124	-0.058	-0.071	17.943	-22.613	-1.682	0.505	-7.515	2.730	-5.758
4.800	3.000	0.210	0.190	0.164	-0.005	0.096	16.666	-18.652	2.681	-1.141	-8.095	2.500	-6.584
4.800	3.050	0.210	0.138	0.119	-0.003	0.071	17.228	-20.070	-0.610	0.569	-7.585	2.155	-6.800
4.800	3.150	0.210	0.036	0.027	-0.019	0.015	0.865	-0.693	0.025	-0.011	-0.530	0.162	-0.506
4.900	2.850	0.210	0.139	0.110	-0.076	-0.035	7.583	-8.236	0.223	-0.031	-4.101	0.990	-2.830
4.900	2.900	0.210	0.071	0.056	-0.035	-0.026	6.462	-7.012	0.101	0.842	-3.157	0.674	-2.754
4.900	3.000	0.210	0.049	0.040	0.014	0.025	7.048	-7.781	1.264	-0.731	-3.031	0.846	-3.285
4.900	3.050	0.210	0.131	0.109	0.051	0.051	6.581	-6.928	0.413	-0.754	-3.522	0.555	-2.712
4.900	3.150	0.210	0.042	0.030	0.009	0.028	1.718	-1.228	0.043	-0.103	-1.388	0.081	-0.820
4.950	2.850	0.210	0.073	0.049	-0.054	-0.010	5.117	-5.270	0.630	0.365	-2.708	0.451	-2.255
4.950	2.900	0.210	0.011	-0.007	-0.005	0.006	5.898	-5.716	-0.055	0.429	-2.816	1.363	-3.265
4.950	2.950	0.210	0.030	-0.016	0.003	0.026	4.165	-3.489	0.458	0.747	-2.232	0.621	-2.609
4.950	3.000	0.210	0.031	0.003	0.015	0.027	4.494	-4.087	0.734	0.164	-2.239	0.533	-2.663
4.950	3.050	0.210	0.074	0.041	0.053	0.033	4.857	-5.322	0.016	-0.157	-2.084	0.451	-2.309
4.950	3.150	0.210	0.101	0.035	0.089	0.033	3.163	-2.761	0.236	-0.196	-2.113	0.374	-1.453
4.600	2.200	0.210	0.023	0.004	0.018	-0.015	0.423	-0.284	0.105	0.099	-0.276	-0.092	-0.287
4.600	2.400	0.210	0.027	0.007	0.021	-0.016	0.507	-0.257	0.120	0.081	-0.464	-0.155	-0.293
4.600	2.600	0.210	0.037	0.019	0.004	-0.032	0.654	-0.468	0.176	0.185	-0.406	-0.224	-0.434
4.600	3.500	0.210	0.043	0.030	-0.031	0.005	0.049	-0.026	-0.006	0.003	-0.034	0.003	-0.039
4.600	3.700	0.210	0.027	0.015	-0.022	0.000	0.118	-0.077	0.020	0.012	-0.080	-0.022	-0.079
4.700	2.200	0.210	0.021	0.006	0.019	0.005	0.549	-0.345	-0.027	0.010	-0.400	-0.039	-0.353
4.700	2.400	0.210	0.035	0.018	0.029	0.005	0.373	-0.225	0.076	0.008	-0.273	-0.015	-0.247
4.700	2.600	0.210	0.043	0.023	0.036	-0.008	0.591	-0.407	0.009	-0.021	-0.444	-0.201	-0.332
4.700	3.500	0.210	0.037	0.027	-0.021	0.013	0.360	-0.298	0.065	0.028	-0.186	-0.085	-0.236
4.700	3.700	0.210	0.021	0.016	-0.013	0.003	0.079	-0.067	0.011	0.002	-0.036	-0.011	-0.054
4.800	2.200	0.210	0.016	0.012	0.007	0.008	1.019	-0.818	-0.003	-0.005	-0.620	-0.064	-0.601
4.800	2.400	0.210	0.032	0.025	0.010	0.016	1.024	-0.845	-0.132	-0.036	-0.592	-0.145	-0.611
4.800	2.600	0.210	0.038	0.024	0.029	0.008	0.465	-0.309	-0.048	-0.043	-0.342	-0.032	-0.280
4.800	3.500	0.210	0.024	0.017	-0.003	0.016	0.775	-0.664	0.109	-0.057	-0.499	-0.153	-0.386
4.800	3.700	0.210	0.013	0.013	0.002	0.004	0.446	-0.294	0.085	-0.014	-0.321	-0.138	-0.276
4.900	2.200	0.210	0.019	0.010	-0.014	0.008	1.153	-0.943	-0.258	-0.090	-0.866	-0.012	-0.495
4.900	2.400	0.210	0.018	0.015	-0.008	0.004	1.169	-0.931	-0.101	-0.076	-0.751	-0.081	-0.655
4.900	2.600	0.210	0.018	0.014	-0.006	0.010	1.537	-1.299	-0.294	-0.117	-1.080	-0.203	-0.696
4.900	3.500	0.210	0.017	0.012	0.010	0.008	1.457	-1.239	0.117	-0.183	-0.884	-0.393	-0.791
4.900	3.700	0.210	0.023	0.010	0.020	0.005	1.419	-1.211	0.315	0.120	-0.874	-0.495	-0.754
4.950	2.200	0.210	0.038	0.003	-0.038	0.006	1.588	-0.970	-0.206	-0.040	-1.325	-0.419	-0.880
4.950	2.400	0.210	0.046	0.009	-0.045	0.004	1.514	-1.077	-0.446	-0.019	-1.235	-0.117	-0.716
4.950	2.600	0.210	0.076	0.011	-0.075	0.004	2.205	-1.587	-0.487	-0.065	-1.697	-0.316	-1.126
4.950	3.500	0.210	0.052	0.003	0.049	0.015	1.595	-1.207	0.518	0.067	-1.275	-0.302	-0.707
4.950	3.700	0.210	0.040	0.003	0.039	0.008	1.049	-0.707	0.237	-0.005	-0.831	-0.287	-0.561
3.800	2.750	0.210	0.016	0.014	0.007	0.001	0.008	-0.005	0.002	0.000	-0.006	-0.001	-0.004
3.800	3.300	0.210	0.012	0.012	0.002	-0.001	0.003	-0.003	-0.001	0.000	-0.002	-0.001	-0.002
3.900	2.750	0.210	0.019	0.016	0.011	0.000	0.015	-0.009	0.002	0.001	-0.009	-0.001	-0.013
3.900	3.300	0.210	0.009	0.009	-0.001	-0.002	0.003	-0.003	-0.001	0.000	-0.002	-0.000	-0.001
3.950	2.750	0.210	0.021	0.018	0.011	-0.001	0.013	-0.008	0.002	0.000	-0.006	-0.003	-0.011
3.950	3.300	0.210	0.008	0.007	-0.002	-0.002	0.006	-0.004	-0.001	0.000	-0.003	-0.001	-0.005
4.600	2.750	0.210	0.028	-0.002	0.019	-0.020	0.792	-0.656	0.079	-0.011	-0.390	-0.171	-0.537
4.600	3.300	0.210	0.035	0.014	-0.019	-0.025	0.512	-0.268	-0.034	0.044	-0.423	-0.069	-0.332
4.700	2.750	0.210	0.037	0.002	0.036	0.004	0.478	-0.273	-0.043	0.003	-0.374	-0.065	-0.308
4.700	3.300	0.210	0.044	0.021	-0.038	0.008	0.358	-0.218	-0.006	0.085	-0.280	-0.035	-0.218
4.800	2.750	0.210	0.029	0.010	0.027	0.007	1.226	-0.861	0.076	-0.005	-0.925	-0.377	-0.667
4.800	3.300	0.210	0.029	0.013	-0.020	0.017	0.678	-0.561	0.040	-0.033	-0.382	-0.174	-0.413
4.900	2.750	0.210	0.068	0.045	-0.050	-0.008	3.644	-2.429	0.065	0.075	-3.175	-0.833	-1.683
4.900	3.300	0.210	0.024	0.009	0.013	0.018	1.010	-0.749	0.246	-0.125	-0.707	-0.174	-0.564
4.950	2.750	0.210	0.102	0.037	-0.095	-0.003	3.646	-3.232	0.100	0.304	-2.528	-0.496	-1.532
4.950	3.300	0.210	0.068	0.002	0.063	0.025	3.737	-2.497	1.228	0.625	-3.024	-1.584	-1.953